CALIFORNIA STATE UNIVERSITY, NORTHRIDGE

Structure and Geomorphology of West Whitewater Hill, a Compressive Stepover between the Banning and Garnet Hill Strands of the San Andreas Fault, Whitewater, CA

A thesis submitted in partial fulfillment of the requirements

For the degree of Master of Science in Geology

By

Brittany Elaine Huerta

May 2017

The thesis of Brittany Elaine Huerta is approved by:

Richard Heermance Ph.D.	Date
Julian Lozos Ph.D.	Date
J. Douglas Yule Ph.D., Chair	Date

California State University, Northridge

ACKNOWLEGEMENTS

I would like to express my immense gratitude for Dr. Doug Yule for all of his suggestions, help, understanding, and patience with my project and especially the writing process. I would also like to thank Dr. Richard Heermance and Dr. Nat Lifton, their suggestions and insights that were invaluable to this project. Thank you to Doug Yule, Richard Heermance and Julian Lozos for their valuable, timely, and considerate feedback on my thesis and for their help throughout this whole process.

Thank you to the Geological Society of America (GSA), CSUN Graduate Research Studies department, Marilyn Hanna, and the CSUN Geology department for financial support while earning my Master's degree.

At this point I am grateful to be able to acknowledge all of the support, encouragement, and consideration shone to me by Dr. Judy Schmidt-Levy from the UCS on campus. Words cannot describe.

DEDICATION

Doug, this is for you. You're the best advisor I could have ever asked for. No one could have encouraged and pushed me through my insecurities and fears like you have. Secondly, this thesis is dedicated to my family and friends, they supported me throughout the entire process of my project and I cannot thank them enough for their love.

TABLE OF CONTENTS

LIST OF TABLES

LIST OF FIGURES

ABSTRACT

Structure and Geomorphology of West Whitewater Hill, a Compressive Stepover between the Banning and Garnet Hill Strands of the San Andreas Fault, Whitewater, CA

By

Brittany Elaine Huerta

Master of Science in Geology

The possibility of a large San Andreas Fault (SAF) earthquake that ruptures a 300 km-long reach of the fault from the Coachella Valley to the Mojave Desert (2008 ShakeOut Scenario earthquake) has focused attention on the structurally complex San Gorgonio Pass (SGP) region, which may inhibit this type of quake. Fault strands that comprise the SAF system here are characterized by slip-rate gradients and slip transfer from one strand to another that can allow SAF earthquakes to carry through the pass region. This report focuses on the structure and geomorphology of West Whitewater Hill

(WWH) which occupies the 2.5 km-wide compressive left stepover between Banning and San Gorgonio Pass Fault Zone-Garnet Hill strands of the SAF. WWH is an actively growing, south-plunging, open anticline cut by secondary N- and NW-striking reverse faults. The top of WWH is capped by a distinct orange-red soil developed on a mid-late Pleistocene (230-120 ka) fan surface (F1). This horizon serves as a strain marker that helps to define the structural relief between the two faults, and possible dextral offset along the Banning strand. Underlying the F1 surface is a fanglomerate unit (Qf2) that is beheaded from its source in Whitewater Canyon and appears to have been dextrally offset by 1.5-2.7 km, and yields a maximum dextral slip rate on the Banning strand of 7.0-23 mm/yr since 230-120 ka. This late Pleistocene rate is higher than the Holocene rate of 4-6 mm/yr reported by previous work and suggests that the motion on the Banning strand may have slowed. Folding of the F1 surface at WWH gives shortening and uplift rates of 1.5-3.3 mm/yr and 1.6-3.7 mm/yr, respectively. The shortening occurs parallel to the Banning and Garnet Hill (GH) strands, SAF and can account for ~half of the ~5 mm/yr of dextral slip that transfers between them at WWH. The structure and geomorphology of WWH therefore documents slip transfer between the Banning and Garnet Hill strands and helps to explain how slip on the San Andreas Fault is transferred through the structurally complex San Gorgonio Pass.

INTRODUCTION

Understanding the slip rates and structures in the San Gorgonio Pass (SGP) has important implications for hazard assessment in southern California (e.g., Sykes and Seeber, 1985; Yule and Sieh 2003; Jones et al., 2008; Heermance and Yule, in press). One debate centers on whether a San Andreas rupture can break through the largest structural knot along its 1100-km length at a 20 km-wide compressive left stepover centered at SGP (Figure 1). If this complexity inhibits rupture, then SAF earthquakes will likely be contained to either side, and smaller in magnitude. Alternatively, a rupture that starts within, or propagates through the SGP can potentially involve a >300-km length of the fault and may produce a M7.9 quake (2008 ShakeOut Scenario earthquake; Jones et al., 2008).

The hazard posed by faulting in San Gorgonio Pass is of particular interest to southern California for several reasons. Numerous infrastructure elements that pass along the Interstate 10 corridor here are at risk from rupture and strong ground shaking (Figure 1 and 2). For example, the Colorado River Aqueduct passes directly beneath West Whitewater hill and crosses all SAF related structures here including the Banning and Garnet Hill strands as well as the folds and faults within the stepover. Repair of the aqueduct after a large earthquake will depend on the magnitude of offset (Weldon et al., 2016). Other infrastructure elements include ~ a hundred wind turbines atop WWH and surrounding areas, numerous power lines owned by Southern California Edison, buried high-pressure gas lines and optic cable, freight rail lines, and Interstate 10 itself are also at risk from surface deformation here.

The structural complexity of the pass region owes its origin to the oblique collision of the San Jacinto and San Bernardino Mtns blocks, and presents a formidable challenge to resolving the debate whether large SAF earthquakes can carry through the pass (Figure 1) (e.g., Allen, 1957; Morton and Matti, 1993; Yule and Sieh, 2003). Structures in the SGP are fed from the northern Coachella Valley (to the east) by a left-stepping system of dextral-slip faults, the Mission/Mill Creek, Banning, and GH strands, and from the San Bernardino region by the San Bernardino strand (Figure 1). Structures within the pass are dominated by a left-stepping system of dextral strike-slip and thrust faults referred to as the San Gorgonio Pass Fault Zone (SGPFZ) (Matti et al., 1982; 1993; Yule and Sieh, 2003). The 2.5 km-wide stepover between the Banning and GH strands centered at WWH is the focus of this report. The objective is to gather information about the structure and geomorphology of WWH by making a detailed geologic map and using known ages to constrain uplift and shortening rates of WWH and a dextral slip rate on the Banning strand. The results show that WWH is uplifting at 1.5-3.3 mm/yr and shortening at 1.6-3.7 mm/yr in a direction parallel to the Banning and GH strands. The uplift and shortening rates are ~half of the ~5 mm/yr slip rates on the fault strands outside of this stepover and document deformational structures in WWH that transfer motion between the Banning and GH strands (Gold et al., 2015; Heermance and Yule, in press). For example, the Banning strand SAF moves at an average rate of ~5 mm/yr to the north of Palm Springs and appears to slow to the west and stop moving altogether at the longitude of Cottonwood Canyon (Yule and Sieh, 2003; Gold et al., 2015). In contrast, the GH strand is moving slowly, if at all, to the north of Palm Springs and speeds up to the west

where it moves at an average rate of ~5 mm/yr in SGP (Heermance and Yule, in press). The slip rate gradients on the sub-parallel Banning and SGPFZ-GH strands therefore appear to mirror each other. The data and results therefore help explain how slip transfer occurs in the pass region, which may allow for large-magnitude events to break the SAF for long distances on both sides of the SGP.

GEOLOGICAL BACKGROUND

Evolution of the San Andreas Fault at the San Gorgonio Pass

The San Andreas Fault system in the SGP region has reorganized a number of times since the Pliocene (Matti et al., 1982; 1993). The reason for the instability of the fault here is not well known but probably relates to a combination of several factors including interaction with the Pinto Mountain Fault (Kendrick et al., 2015), heterogeneity in the mid- to deep-level of the crust (Langenheim et al., 2005), and oblique collision between the San Jacinto and San Bernardino Mountains blocks (e.g., Seeber and Armbruster, 1995; Yule and Sieh, 2003; Carena et al., 2004) (Figure 1). Paleogeographic reconstructions describe how the SAF system has changed in the SGP region: a) the Mission Creek strand with ~130 km of total dextral offset shut down by ~500 ka; b) the Mill Creek strand with ~8 km of total offset shut down at ~150 ka; and c) the San Bernardino, SGPFZ-GH, and Banning strands represent primary active strands today (Matti et al., 1982; Matti et al., 1993; Yule and Sieh, 2003) (Note that the Mission and Mill Creek strands merge into a single Mission/Mill Creek strand in the Coachella Valley) (Figure 1). Interestingly, mechanical models show that the recent configuration of the fault system provides a relatively inefficient path for San Andreas motion to carry through the Pass (Cooke and Dair, 2011; Herbert and Cooke, 2012).

Late Pleistocene to Holocene Slip Rates

Slip rates along the San Andreas system vary along strike and reach a minimum in the SGP region (e.g., McGill et al., 2013; Heermance and Yule, in press). Outside of the pass region, the San Andreas system moves at 7-16 mm/yr near San Bernardino

(McGill et al., 2013) and at 12-22 mm/yr near Indio (Behr et al., 2010) and 22-26 mm/yr at Pushawalla Canyon (Blisniuk et al., 2013). Faults move at 4-8 mm/yr within the pass region (Gold et al., 2015; Heermance and Yule, in press). Slower rates in SGP may reflect slip transfer to the San Jacinto and/or the Eastern California Shear Zone to the west and east of the pass, respectively. In addition, slip may follow a northern path through SGP (Morelan et al., 2016). Another hypothesis is that some of the missing slip is occurring as off-fault, diffuse deformation in the eastern SGP region and Little San Bernardino Mtns (Fattaruso et al., 2016).

At WWH, the Banning strand, SAF has been reactivated in the late Pleistocene and juxtaposes crystalline rocks of the San Gabriel terrane against Pleistocene Cabezon fanglomerate (Allen, 1957; Matti et al., 1993). This most recent motion on the Banning strand has produced ~2 km of right-lateral slip, but isn't regarded as the dominant strand of the SAF (Gold et al., 2015). Here, Gold et al. (2015) used geomorphology, B4 LiDAR, geochronology, and alluvial fan reconstruction to find a slip rate of 4-6 mm/year. To the southwest and southeast of this site the GH strand shows surface expression, but little is known about this strand or how much slip is being partitioned onto it from the Banning. The GH strand can be hypothesized to move ~2 mm/yr so that the combined rates of the GH plus Banning strands equal the 4-8 mm/yr rate observed on two splays of the SGPFZ at Millard Canyon in SGP (Heermance and Yule, in press).

The GH strand of the SAF is thought to be a reverse fault or right-reverse fault (Yule and Sieh, 2003) (Figure B7). At WWH the GH strand consists of a single splay to the southeast and three splays in the northwest (Figures 1 and 2). The northern splay

shows a possible right-lateral offset of 15 to 100 meters, and the southern splay appears to be mostly reverse slip, with a maximum scarp height of about 1.5 meters, and an average of <1 m (Figure B2). Between the Banning and GH strands there is an area of sharp relief where the Banning strand takes a left step to the Garnet Hill strand and the sediments consist of uplifted fluvial and alluvial fans (Figure B4). The structures seen here are at least surficially similar to the structures observed between the Mission Creek and Banning strand where a left step-over takes place between the two faults to the southeast of West Whitewater Hill (Gold et al., 2015).

METHODS

Field Mapping

We completed field mapping on a DEM base map generated from B4 LiDAR data and obtained through *opentopograpgy.org*. We identified prominent, well-indurated, and color unique layers (interpreted to be paleosols) in the study area and traced them throughout the region (Figure B4 and B5). Outcrops are confined to six main deeply incised canyons. We used Google Earth to supplement the DEM maps, to mark points and measurement locations. We identified fault scarps along the southern splay of the Garnet Hill strand first on the DEM maps (Figure B2) and then followed on foot until surface expression could not be found, with several scarp height measurements taken in the process using a tape measure.

Strike and dip measurements were difficult to obtain due to the often two-dimensional nature of outcrops. In most cases we took two trend and plunge measurements from layering at outcrop faces at each location and plotted them to determine strike and dip of layering (Stereonet 8, Allmendinger et al., 2013) (Appendix A). We also used this method to generate paleocurrent directions where possible. We entered raw trend and plunge measurements that were then plotted on a digital stereonet. We used the stereonets to calculate strike and dip measurements from the combination of multiple trend and plunges plotted in the same circle.

Clast counts

We recorded four clast counts in and around WWH; of those, two were from the active Whitewater River and Cottonwood Canyon, while the other two were from

outcrops specifically in unit Qf1 (Figure 2, black triangles). The clast sizes range from coarse sand to boulders. We counted the clasts along a 5-m line of measuring tape directly in the washes and pinned to the outcrops. We took the counts every 10 cm to make the count unbiased. The initial clast count contained matrix points, but later we decided to pick the closest clast to a matrix point. I chose to omit the matrix from the clast counts because I wanted to know the relative abundances of clasts and possibly identify a source for these clasts. This information can help determine, for example, whether the alluvial fans have been displaced from their sources via lateral slip on the Banning strand SAF.

Stratigraphic Columns

We produced five stratigraphic columns from the geologic map in steep canyons (locations shown in Figure 2). Within these canyons the walls were too steep to measure the thicknesses directly, so we approximated the thicknesses using elevation differences. To get as close to a true stratigraphic thickness as possible we took most of the columns from west and southwest or east and northeast facing walls at a high angle to strike. In the one or two cases where the columns are taken from a low strike angle, the low dip of the strata (10-20 degrees) causes a minor (<10%) overestimation of thicknesses. Five separate units were identified within WWH, one of them being Qf2 (Figure 9 and 10).

^{26}Al/^{10}Be Cosmogenic Nuclide Isochron burial dating

I helped my collaborator Dr. Nathaniel Lifton (Purdue University) collect samples for isochron burial age-dating analyses at three locations (Figure 2, black circles; Figure B1). This relatively new dating method is being tested at Dr. Lifton's lab. This method

measures decay products of cosmogenic radionuclides (^{10}Be and ^{26}Al) that collect in cobbles after they are buried. The relative abundances of each isotope can produce an isochron whose slope can give an age since burial (Erlanger et al., 2012). Sample specimens include clasts with high quartz content taken from the units we want to constrain the ages of, we targeted paleosols to maximize ^{26}Al/^{10}Be concentrations. Al concentrations and isotope ratios of Al and Be were measured using an accelerator mass spectrometer.

Certain factors can change the age outcome if they aren't input into the CRONUS calculator correctly. These factors include: elevation above sea level, latitude and longitude coordinates, and the depth below the surface the clasts were collected from. All age dating methods have their drawbacks and this method is no different in that regard. Assumptions need to be made to calculate ages using burial dating techniques, some of those assumptions are that the clasts being dated have only been buried once and if the nuclide accumulation rate is faster than 10 cm/kyr, then the burial age can be insensitive to the assumption of steady accumulation (Balco et al., 2013). Uncertainties in the final age can be attributed to the fit of the isochron line, analytical error of the accelerator mass spectrometer (AMS), uncertainty in the measured ^{26}Al/^{10}Be ratio when multiplied by the mean life of burial, and the uncertainties of radioactive mean lives and the production rate ratios. To date only one sample has been analyzed and two are still being processed.

Uplift, shortening, and dextral slip rates

Estimates for uplift and shortening rates across WWH were determined for both an east-west (Figure 6) and north-south (Figure 7) cross section of the hill. We divided

these estimates by age estimates from published age estimates based on soil development (Kendrick et al., 2015), interglacial periods, and an age range of PS1 from N. Lifton (in progress). We determined shortening by the change in line-length between the deformed fan surface ($l_{original}$) today and the present-day horizontal distance (l_{final}) (Figure B8). We determined uplift by the change in height between the deformed fan surface (z_2) today and base level (z_1), where modern fans are forming. We measured the differences in line-length changes parallel to the Banning strand (Figure 6) and perpendicular to faulting (Figure 7). We divided the changes by the estimated age data from the dating techniques described above.

RESULTS

Introduction

Figure 2 includes a variety of rock units including a late Proterozoic through late Mesozoic igneous and metamorphic complex of primarily gneiss and granodiorite, and middle Pleistocene through Holocene alluvial fan deposits. The Banning strand of the SAF juxtaposes the crystalline rocks against the sedimentary rocks. Transpression between the Banning strand and the Garnet Hill strands of the SAF has uplifted, folded, and faulted the Pleistocene alluvial fan deposits.

Crystalline Rock Units

The oldest map unit in the area is the Precambrian to Cretaceous mylonitic and foliated granitic rocks (PcK) also known as the San Gabriel Mountains crystalline basement terrane (Kendrick et al., 2015). These rocks range in color from grey and black to blue and green. The southern limit of this unit is a relatively nonresistant, valley-forming fault breccia and gouge zone along the Banning strand of the SAF (Figure 4). A prominent soil (Qs) has formed on the low-relief, upland areas of this unit (Figure 2) at the ~same elevation as the soil atop of WWH suggesting that little uplift has occurred across the Banning strand since the soil began to form (Figure 2).

Stratigraphic Units

General

West Whitewater Hill exposes over 400 m of alluvial fan material, but it can be sub-divided into members based on my mapping of paleosols within this section. In the

following text I have adopted some of the nomenclature published by Owen et al. (2014) for consistency.

Cabezon fanglomerate

WWH is now densely covered with wind turbines and is underlain by the Cabezon fanglomerate as first defined by Vaughan (1922) and later by Allen (1957). Owen et al. (2014) subdivided the Cabezon fanglomerate here into Fans 1 and 2 equivalent to units Qf1 and Qf2 on Figure 2. Exposures in deeply incised canyons of Whitewater Hill, and in outcrops on the east wall of Whitewater Canyon, reveal a prominent paleosol (PS1) that separates Qf1 from Qf2.

Qf1. Qf1 is the bottom-most exposed unit within WWH. The exact thickness of the unit is unknown. The top of Qf1 is defined by a moderately to well-developed, well-cemented, orange-yellow paleosol (PS1), and described in Figure 3. The clasts that make up the conglomerate consist of subangular to subrounded igneous, metamorphic, volcanic, and rare sedimentary rocks. The matrix consists of sand to coarse pebbles.

Results of two clast counts from unit Qf1 are shown in Figure 8 (black triangles on Figure 2). Unit Qf1 consists predominantly of granitic clasts, in particular granites with high concentrations of quartz and feldspars. Intermediate in abundance are varieties of gneiss including epidote-rich, felsic gneiss, and diorite gneiss clasts. The least common clast types are volcanic rocks including andesite porphry and basalt, seen in only one clast count towards the center of West Whitewater Hill. The rarest clast type, and one of the more important, is piemontite-bearing quartzite. Piemontite is a purplish-red epidote-group that is part of a distinctive clast type from Qf1 (and also noticed as loose float in

unit Qf2) that only outcrops with the San Gabriel terrane to the north of WWH in the canyon walls of the modern Whitewater River. The presence of piemontite-rich quartzite, volcanic, and sandstone clasts in unit Qf1 (and also Qf2) indicate that the ancestral Whitewater River deposited this unit. Clasts from Qf1 are similar to the modern alluvium counted in the modern Whitewater River.

Within Qf1 there are occasional well-defined fining upward beds (Figure B3) that range in thickness from 3 to 30 cm thick. In these small sequences the clasts run from gravels near the base to pebbly coarse sand at the top. From these we were able to record two paleocurrent directions using the weak imbrication observed from the larger clasts at the base of the sequence. There were only two paleocurrent measurements taken; one flow direction was almost due south, the other was south-southwest.

Qf2. Unit Qf2 overlies unit Qf1 and forms the upper 50-130 m of the section exposed at WWH (Figure B5). The unit is capped by a soil (unit Qs). Within Qf2 a second paleosol (PS2) is present, but is discontinuous and is most extensive in the eastern part of the study area. The thickness of Qf2 varies from 50-130 meters (Figures 9, 10, and 11). Unit Qf2 itself is composed mainly of a poorly-sorted, moderately-indurated, greyish-buff colored, clast-supported cobble conglomerate. The matrix between the clasts ranged from silt to coarse sand. Clast sizes began at pebbles and range up to boulders, some greater than a meter in width. Clast counts were not taken from Qf2 because outcrops of the member were typically on cliff faces making reaching them unsafe.

The thickness of unit Qf2 across the study area is shown in Figures 9, 10, and 11. Figure 2 is used to estimate the thicknesses of unit Qf2 by measuring the elevation

difference between the top of paleosol 1 (PS1) and the late Pleistocene terrace (Qs). The elevation differences are a close approximation of thickness where strike of bedding is at a high angle to the cliff exposures, but overestimates the thickness by ~5% where strike is parallel to the cliff exposure, which is uncommon in the field area. Because the correction is negligible, Figures 9 and 10 do not include a correction for any possible overestimate of thickness. Contours of the thickness estimates show a slightly asymmetric fan shape with an apex that is beheaded by the Banning strand in the middle of West Whitewater Hill (Figure 11). The axis of the fan trends south-southeast and is similar in shape and relief to the active fan that now exists at the mouth of the modern Whitewater River Canyon (Figure 12). Qf2 therefore probably represents a late Pleistocene Whitewater River fan deposit whose crest has shifted 1.6-2.7 km to the west due to slip on the Banning strand (Figure 11).

Alluvium

Qaf, Qau. Areas of low relief at low elevations contain late Pleistocene and Holocene alluvium (Figure 2). Clast counts were collected in two places, in the active washes of Whitewater and Cottonwood Canyons (Figure 13) and show that alluvium deposited from modern Whitewater River is distinct from alluvium deposited from Cottonwood Canyon deposit.

Alluvium here is divided into two types: faulted alluvium (Qaf) with scarps that range from 1 to 10 m high, and unfaulted alluvium (Qau) with no scarps. Deposition of unfaulted alluvium is thought to post-date the most recent rupture here. The timing of the most recent rupture here is unknown, but could have possibly happened about 600 years

ago due to evidence of a 600-year-old rupture excavated in paleoseismic sites both north and south of the SGP (e.g. Scharer et al., 2013; Yule et al., 2015).

Granite was the predominant clast type found in all of the canyons, followed by biotite schist, and diorite/hornblende granite. While all of the canyons contained similar igneous and metamorphic clast types, there were two significant differences between Whitewater River and Cottonwood Canyon (Figure 13). First, volcanic clasts are present in the modern Whitewater River. Second, the clasts from Cottonwood Canyon had higher levels of mafic minerals. Clast counts from Qf1 are more similar to Whitewater River alluvium than they are to Cottonwood Canyon alluvium.

Structure

Faults

Banning Strand, San Andreas Fault. The Banning strand SAF juxtaposes crystalline rocks against units Qf1 and Qf2. The fault is west-striking, and dip changes from steep (75 degrees N) east of Whitewater Canyon, to moderate (45 degrees N) immediately west of the canyon, to shallow (<15 degrees N) and locally shallowly south-dipping at Cottonwood Canyon (Figure 2). Thick vegetation within young alluvium of Whitewater Canyon abruptly ends at the fault. A thick zone of cataclasite and gouge characterize the crystalline rocks adjacent to the fault (Figure 4). Uphill facing scarps within the units Qf1 and Qf2 locate the fault zone in a tributary of Cottonwood Canyon on the north slope of West Whitewater Hill.

Garnet Hill Strand, San Andreas Fault. Overall, the GH strand strikes west (Figure 2). It is presumed to dip north but no direct observation can confirm this. The GH

strand is a single strand where it crosses Whitewater River. Here an 8-10 m-high, up-on-the-north scarp is expressed in Qaf immediately to the west of the river. The GH strand splits into two splays (north GH and south GH) about 1 km west of Whitewater River.

The south splay is expressed in unit Qaf as an ~1 m-high, up-on-the-north scarp. In places, Qau has buried this scarp. North splay shows up-on-the-north and right-lateral offsets. Evidence for lateral motion includes deflected drainages with 15-30 m of dextral offset, and a truncated terrace riser with 60-100 m of dextral offset (Figure 14). The lateral offsets displace unit Qaf. Uplift of Qs in the fault's hanging wall provides evidence for vertical motion. Fault motion has uplifted this surface by 250-400 m, although this motion is likely a product of both up-on-the-north slip on the GH strand and folding (Figures 2, 6, and 7).

The northern GH fault breaks into two more splays as it crosses Cottonwood Canyon wash. To the west of this wash, the two north GH splays continue west, but are known as the San Gorgonio Pass Fault System that shows right-lateral and reverse motion along the trace. Young alluvial fan deposits sourced by Deep Canyon bury the southern GH splay (Deep Canyon is to the west of Cottonwood Canyon).

Secondary faults. Two unnamed north and north-northwest striking faults connect the Banning and GH faults (Figures 2, 5, 6, and 7). The western fault offsets paleosol 1 with about 50 m of vertical offset (up on the east, Figure 7). It also offsets the late Pleistocene terrace remnant by the same amount. A log of the boring of the Colorado River Aqueduct shows a 75 degree east-dipping fault whose up-dip projection would intersect the map trace of this fault (Weldon et al., 2016). This secondary fault is

therefore considered to be a reverse fault. The eastern fault has a complex surface trace (Figure 5) that has been simplified on Figure 2. Numerous small scarps, all up on the east, are found along the trend shown on the map. This complex fault offsets Qs in total by about 20 m, up on the east, but loses surface expression toward the north. It may be another reverse fault. Alternatively, it may be a landslide scarp (Matti et al., 1982).

Fold

Bedding within the units Qf1 and Qf2 define an open, gently south-plunging fold hinge to the west of the north-south secondary fault (Figures 2, 6, and 7). The orientation of layering on the east limb strikes north to northeast and dips 12-25 degrees east and southeast. Layering on the west limb is not well exposed but where observed strikes west to northwest and dips 5-15 degrees to the south and southwest. The fold hinge plunges ~10 degrees to the south.

The fold amplitude is a proxy for uplift because it is a deformed fan surface. To the first order, the fold amplitude can be estimated by comparing the elevation in Figures 6 and 7. Along section A-A' (Figure 6), relief at the level of Qs is ~350 m, with a maximum elevation of ~850 m at the center of WWH and ~500 m at the west and east edge of the hill. Along section B-B' (Figure 7), relief at the level of Qs surface is ~400 m, with a maximum elevation of ~800 m at the center of WWH and ~400 m at the south edge of the hill (across the south splay of the Garnet Hill strand). However, the topographic relief does not take into consideration the paleo topography (see Geomorphology, below). The fold in section A-A' can also be used to estimate the

amount of shortening across the fold, and is ~400 m ($l_{orignal} - l_{final}$ =400 m) by subtracting the horizontal distance (l_{final} = 5.40 km) from the line length along Qs ($l_{original}$ = 5.80 km).

Geomorphology

We mapped three alluvial fan surfaces (F1-F3) in the study (Figure 15). We interpret them to record fan abandonment in response to tectonic uplift with subsequent incision and establishment of new fans that are inset into the previous fans. The oldest fan surface (F1) is found at the highest elevations and is the most extensive in the study area. F1 is characterized by a deeply weathered orange-red soil (Qs) and is the fan surface that caps unit Qf2 (Figure 2). F1 corresponds to fan surfaces Fw2 and Fw3 of Owen et al., 2014. The original relief across this fan surface is estimated to be ~30 m, similar to the relief on the modern fan that emanates from Whitewater Canyon (Figure 12). This original relief of F1 means that uplift during folding is estimated at 370 ± 30 m (Table 3).

Younger fan surfaces occur in Whitewater and Cottonwood canyons and in low-relief areas to the south of Whitewater Hill. Fan surfaces F2 and F3 have weak soils and cap units Qaf and Qau, respectively. F2 corresponds to fan surfaces Fw4 and Fw5, and F3 corresponds to fan surfaces Fw6 of Owen et al., 2014. These fan surfaces range in age from modern (F3/Fw6) to ~80 ka (F1/Fw2-3) (Owen et al., 2014).

Ages

A compilation of age data discussed below is given in Table 2. Data are from Owen et al., 2014; Kendrick et al., 2015, and N. Lifton (personal communication).

Qf2. N. Lifton has initiated a project to determine burial ages of soils and paleosols in the study area. Preliminary burial age data from PS1 (paleosol atop unit Qf1)

suggest that it is 330-510 ka (Lifton, personal comm.). The age of Qs (F1) must be younger. Until recent years the ability to collect samples that give reliable age data that agrees with the assumed age of the soil has been difficult to collect in this area. The lack of data is most likely due to the climate, high winds, and clast size making the usual surficial dating processes difficult at best. Burial age analyses of samples collected from ~10 m beneath unit Qs are currently being processed. Until a burial age can be obtained, we think that Qs most likely developed during isotope 8-7 transition at 230 ka or isotope 6-5 transition at 120 ka. The latter is consistent with a preferred soil age of 106-130 ka for Qs in Kendrick et al., 2015 (their surface C1). In contrast to those ages, Owen et al., 2014 report cosmogenic radionuclide exposure age dates of 40-75 ka from F1 and F2 of this study. Moreover, this 40-75 ka age range is also the age that Owen et al., 2014 assign paleosol 1 (their Fw1) and is an even larger discrepancy in ages (~60 ka vs ~400 ka). We think the Owen et al. 2014 ages are too young for reasons detailed in the discussion. For rate calculations, we use a range of 120-230 ka for the age of the F1 fan surface.

The age data from F3 samples in Whitewater Canyon (Fw4 of Owen et al., 2014) give cosmogenic radionuclide exposure ages of 4.9-6.8 ka. This age range is similar to CRN ages of the Qf3 surface in Millard Canyon (Heermance and Yule, in press). The 4.9-6.9 ka age range from Whitewater Canyon is used in the uplift calculation across the Garnet Hill strand, below.

Rates

The rate estimates for uplift and shortening of the Whitewater Hill are shown in Table 3. The similarity between uplift rates (1.5-3.3 mm/yr) and shortening rates (1.6-3.7 mm/yr) indicate that ~90% of the shortening is expressed as uplift. This is consistent with the fact that large remnants of the F1 surface are preserved across the fold (Figure 15).

The rate of uplift across the Garnet Hill strand is also shown in Table 3. A scarp in F2 is estimated to be 8 +- 1 m. Using Owen's ages for this surface (Fw4) gives an uplift rate of 1.0 – 1.8 mm/yr, in overlap at the low end with the 1.5-3.3 mm/yr late Pleistocene uplift rates.

The isopach map (Figure 11) suggests that the F1 surface atop Qf2 has been dextrally offset by 1.6-2.7 km, equivalent to a dextral slip rate of 7.0-23 mm/yr on the Banning strand of the SAF.

DISCUSSION

Clast provenance

Similarities between the clast compositions and distributions between the modern Whitewater River and unit Qf1 (Figures 8 and 13) support a model where an ancestral Whitewater River was the source for unit Qf1. There are distinct types of clasts that support the hill being made up of Whitewater River-derived sediment. Those clasts are Neogene sandstone, basalt, an andesite porphyry, and piemontite-rich quartzite (a manganiferous epidote). These clasts are common elements in the San Gabriel terrane and outcrop within the narrow Whitewater River gorge that extends ~10 km north from WWH. The distinct clast types mentioned above are not common to the San Bernardino Mtns terrane located to the north of the Mission/Mill Creek strand of the SAF (Figure 1). The presence of San Gabriel terrane clasts throughout the canyons in the hill solidifies the right-lateral offset of the crest of the Qf1 fan and the F1 surface. The offset of the fan is 1.6-2.7 km and yields a slip rate of 7.0-23 mm/yr. The wide range of rates reflects the poor control on offset of the crest of F1 and the large error in age estimation for Qs. The late Pleistocene rates are higher than the Holocene dextral slip rate of 4-6 mm/yr at Painted Hill, just east of WWH (Gold et al., 2015), and suggests that the Banning strand has slowed with time.

Structure

The overall shape of the structure of WWH is a gentle, south-plunging open fold (Figures 2, 6, and 7). This implies east-west oriented shortening, parallel to dextral strike-slip motion on the Banning strand of the SAF. The north splay of the GH strand also appears to be a dextral strike-slip fault (Figure 14). The trend of the WWH anticline is consistent with a structure forming at a left stepover in a right-lateral strike-slip system (e.g., Sylvester and Smith, 1976; McClay and Bonora, 2001). It is interesting to note that this defines a local stress field with maximum shortening oriented ~E-W. This is at odds with the regional stress field which is oriented with maximum shortening ~N-S (Yule and Sieh, 2003). One possibility is that slip transfer between the GH and Banning strands of the SAF is controlling the local stress field. Another possibility is that the difference reflects strain partitioning between largely strike slip and dip slip structural elements in the structurally complex SGP region.

Age dates and Uplift/ Shortening rates

We initially reject Owen's age because TCN boulder dating can have cosmogenic nuclide accumulation problems due to weathering, exhumation, prior exposure, and surface shielding which generally reduces the concentration of TCNs in surfaces. This result is an underestimate of the true age of the landform (Owen et al., 2014). Their range for boulders in F1 was ~40-75 kyr; we reject this age because WWH has been subjected to weathering through strong wind erosion, exhumation, and soil development. Over-exposure of boulders at the surface can also influence younger ^{10}Be ages. For example, we acknowledge that the Kendrick et al. (2015) soil profile age (106-130 ka) of Qs is

closer to the true (minimum) age of fan surface 1. This is because the formation of Qs has to have been at the surface for at least 100,000 to develop its dark red color and thickness. If this surface has been exposed for at least 106 kyr, and as high as 130 kyr (Kendrick et al., 2015), then the ^{10}Be will have reached secular equilibrium essentially stopping the ^{10}Be geologic exposure clock-watch (Matmon et al., 2005). Studies by Pierce and Scott (1982), Ritter et al. (1993), and Gillespie et al. (1994) report that alluvial fans are deposited during glaciation. Soil formation on a fan would mark a period of no deposition or incision allowing the fan surfaces time to develop their soils. With PS1 being between 330-510 kyr and the stratigraphy mapped within WWH (Figure 9), we added the additional restriction of known interglacial periods from the last 520 kyr (Bull, 1991). Figure 9 and 10 shows that PS1 is the oldest paleosol found in WWH, above that is PS2, and the top is capped by Qs (F1 surface). The presence of PS2 means that a second interglacial period may be recorded in the units, if we use the interglacial period that is intermediate to the PS1 age we can conclude that it may have formed during the interglacial period at 410 kyr. We interpret PS2 to be younger than and stratigraphically above PS1 and have assigned it a tentative age of ~330 kyr, which is the next interglacial period younger than 410 kyr. By this reasoning we assign F1 an age range of 120-230 kyr, allowing for a possible formation and erosion of a third paleosol between PS1 and Qs (atop fan F1). We use this age range for F1 to determine uplift, shortening, and a possible dextral slip rates (Table 3).

The presence of a growing hill between these two strands solidifies the theory that slip is being transferred from the Banning strand north of the field area to the Garnet Hill

strands in the south of the field area via a left step-over between two right-lateral faults. The directionality of the strands and the nature of the step-over causes transpressional deformation of the sediment between the two faults, this results in uplift and shortening of a region that was once at base level.

CONCLUSIONS

1. The age of the F1 fan surface at WWH and the initiation of soil formation (Qs) is estimated to correlate with interglacial periods at the isotope 7-8 or 6-5 transitions, at 230 and 120 ka.
2. The crest of the abandoned F1 fan has been right-laterally offset 1.6-2.7 km from its original depositional location at the mouth of Whitewater Canyon. This is supported by similar clast composition of unit Qf1 and the modern river. The preferred age (above) for this surface gives a late Pleistocene slip rate of 7.0-23 mm/yr for the Banning strand of the SAF. Lower Holocene rates indicate that the fault has slowed in recent time.
3. Folding of Qs at WWH give 370 ± 30 m, and 400 ± 40 m of uplift and shortening, respectively, and equivalent to a 1.5-3.3 mm/yr uplift rate and 1.6-3.7 mm/yr shortening rate.
4. The slip-rate gradients known on the Banning and GH strands of the SAF require slip to transfer between them. The shortening rate at WWH anticline documents about 30-70% of the necessary transfer at this compressive stepover.

FUTURE WORK

While this particular thesis is essentially complete it is only a small part of the larger story of the San Gorgonio Pass. In order to develop more precise slip, uplift, and shortening rates a more robust set of age data needs to be generated. Another student could process and analyze the other burial samples at Purdue University for a clearer picture of burial timing. Also, a USGS employee, Devin McPhillips, is interested in looking for possible locations in Whitewater that might allow for dating 3He in iron-oxides. Precise age data is extremely important because the amount of hazard associated with this area and the Colorado River Aqueduct could potentially affect millions of lives in southern California, if it were to break in a large earthquake.

The most recent rupture on the southern splay of the GH strand needs to be dated as well, to determine a possible rupture recurrence interval. Giving the CRA and the Metropolitan Water District some idea of how often and how large ruptures can be in Whitewater, California.

REFERENCES

Allen, C.R., 1957, San Andreas fault zone in San Gorgonio Pass, Southern California: Geological Society of America Bulletin, v. 68, p. 315–350, doi: 10.1130/0016-7606(1957)68 [315:SAFZIS]2.0.CO;2.

Allmendinger, R. W., Cardozo, N. C., and Fisher, D. (2012). Structural Geology Algorithms: Vectors and Tensors: Cambridge, England, Cambridge University Press, p. 289.

Balco, Greg, Soreghan, G. S., Sweet, D. E., Marra, K. R., and Bierman, P. R. (2013). Cosmogenic-nuclide Burial Ages for Pleistocene Sedimentary Fill in Unaweep Canyon, Colorado, USA, *Quaternary Geochronology*, v. 18, p. 149.

Behr, W. M., Rood, D. H., Fletcher, K. E., Guzman, N., Finkel, R., Hanks, T. C., … Yule, J. D. (2010). Uncertainties in slip-rate estimates for the Mission Creek strand of the southern San Andreas fault at Biskra Palms Oasis, southern California. *Bulletin of the Geological Society of America, 122*(9–10), 1360–1377. http://doi.org/10.1130/B30020.1

Blisniuk, K., M. Oskin, A.-S. Mériaux, T. Rockwell, R. C. Finkel, and F. J. Ryerson (2013), Stable, rapid rate of slip since inception of the San Jacinto fault, California, Geophys. Res. Lett., 40, 4209–4213, doi:10.1002/grl.50819.

Cardona, J. E. (2016). *Constraining the most recent surface rupture on the Garnet Hill strand, San Andreas Fault, Coachella Valley, California*. California State University Northridge.

Cardozo, N., Allmendinger, R. W. (2013). Spherical projections with OSXStereonet: Computers and Geosciences, v. 51, no. 0, p. 193 – 205, doi: 10.1016/j.cageo.2012.07.21.

Carena, S., Suppe, J., and Kao, H., 2004, Lack of continuity of the San Andreas fault in Southern California: Three-dimensional fault models and earthquake scenarios: Journal of Geophysical Research, v. 109, B04313, doi: 10.1029/2003JB002643

Cooke, M. L., & Dair, L. C. (2011). Simulating the recent evolution of the southern big bend of the San Andreas fault, Southern California. *Journal of Geophysical Research: Solid Earth, 116*(4), 1–20. http://doi.org/10.1029/2010JB007835

Erlanger, E. D., D. E. Granger, and R. J. Gibbon (2012) Rock uplift rates in South Africa from isochron burial dating of fluvial and marine terraces, *Geology, 40*(11), 1019-1022.

Fattaruso, Laura, Michele L. Cooke, Rebecca J. Dorsey and Bernard Housen, 2016. Response of deformation patterns to reorganization of the southern San Andreas fault system since ca. 1.5 Ma, *Tectonophysics*, doi:10.1016/j.tecto.2016.05.035

Fumal T. E., R. J. Weldon II, G. P. Biasi, T. E. Dawson, G. G. Seitz, W. T. Frost, and D. P. Schwartz 2002. Evidence for large earthquakes on the San Andreas Fault at the Wrightwood, California, paleoseismic site: A.D. 500 to present, Bulletin Seismological Society of America, 92, no. 7, 2726-2760.

Gold, Peter O.; Behr, Whitney; Rood, Dylan; Sharp, Warren; Rockwell, Thomas; Kendrick, Katherine; Salin, A. (2015). Holocene geologic slip rate for the Banning strand of the southern San Andreas Fault, southern California Peter. *Journal of Geophysical Research: Solid Earth*, 1–25. http://doi.org/10.1002/2015JB012004.Received

Heermance, R., et al. (2015) SCEC Annual Conference, Palm Springs, California.

Herbert, J.W., and Cooke, M.L., 2012, Sensitivity of the southern San Andreas fault system to tectonic boundary conditions and fault confi gurations: Bulletin of the Seismological Society of America, v. 102, p. 2046– 2062, doi: 10 .1785 /0120110316.

Holland, H. and Turekian, K. (2014) In Treatise on Geochemistry (2nd Edition). P. 1-35. ISBN: 970080983004. Elsevier, Oxford.

Jones, L.M., Bernknopf, R., Cox, D., Goltz, J., Hudnut, K., Mileti, D., Perry, S., Ponti, D., Porter, K., Reichle, M., Seligson, H., Shoaf, K., Treiman, J., and Wein, A., 2008, The ShakeOut Scenario: U.S. Geological Survey Open File Report 2008–1150, California Geological Survey Preliminary Report 25, version 1.0, 312 p.

Kendrick, K. J., Matti, J. C., & Mahan, S. A. (2015). Late quaternary slip history of the Mill Creek strand of the San Andreas fault in San Gorgonio Pass, southern California: The role of a subsidiary left-lateral fault in strand switching. *Bulletin of the Geological Society of America*, *127*(5–6), 825–849. http://doi.org/10.1130/B31101.1

Lifton, N. A., Bieber, J. W., Clem, J. M., Duldig, M. L., Evenson, P., Humble, J. E., & Pyle, R. (2005). Addressing solar modulation and long-term uncertainties in scaling secondary cosmic rays for in situ cosmogenic nuclide applications, *239*, 140–161. http://doi.org/10.1016/j.epsl.2005.07.001

Lifton, N. A., et al. (in progress). 26Al/10Be cosmogenic nuclide isochron burial dating of samples collected from Whitewater Dome, California.

Matti, J.C., Cox, B.F., Obi, C.M., Powell, R.E., Hinkle, M.E., Griscom, A., and McHugh, E.L., 1982, Mineral resource potential of the Whitewater Wilderness Study Area, Riverside and San Bernardino Counties, California: U.S. Geological Survey Miscellaneous Field Studies Map MF-1478, scale 1: 62,500.

Matti, J.C., and Morton, D.M., 1993, Paleogeographic evolution of the San Andreas fault in Southern California: A reconstruction based on a new cross-fault correlation, in Powell, R.E., Weldon, R.E., II, and Matti, J.C., eds., The San Andreas fault system: Displacement, palinspastic reconstruction, and geologic evolution: Geological Society of America Memoir 178, p. 107–159.

Matti, J.C., Morton, D.M., and Cox, B.F., 1985, Distribution and geologic relations of fault systems in the vicinity of the central Transverse Ranges, southern California: U.S. Geological Survey Open-File Report 85-365, 23 p.

McClay, K., and Bonora, M., 2001, Analog models of restraining stepovers in strike-slip systems, American Association of Petroleum Geologists, v. 85, no. 2, pp. 233-260.

McGill, S. F., Owen, L. A., Weldon, R. J., & Kendrick, K. J. (2013). Latest Pleistocene and Holocene slip rate for the San Bernardino strand of the San Andreas Fault, Plunge Creek, Southern California: Implications for strain partitioning within the southern San Andreas fault system for the last~ 35 ky. Geological Society of America Bulletin, 125(1-2), 48-72. doi:10.1130/B30647.1

Morelan, A., M. Oskin, and M. Valentine (2016), Activity of the Mill Creek and Mission Creek fault strands of the San Andreas fault through the San Gorgonio Pass, in Proceedings American Geophysical Union, San Francisco, CA, 2016, Volume T33D-07

Owen, L. A., Clemmens, S. J., Finkel, R. C., & Gray, H. (2014). Late Quaternary alluvial fans at the eastern end of the San Bernardino Mountains, Southern California. *Quaternary Science Reviews*, *87*, 114–134. http://doi.org/10.1016/j.quascirev.2014.01.003

Philibosian, B., Fumal, T., Weldon, R., 2011. San Andreas Fault Earthquake Chronology and Lake Cahuilla History at Coachella, California. Bulletin of the Seismological Society of America, Vol. 101, No. 1, pp. 13-38

Scharer, K., D. Yule, L. Humbert, and R. Witkosky, (2013), Implications for San Andreas Fault Ruptures based on new evidence from the Cabazon, CA paleoseismic site, San Gorgonio Pass Fault Zone, 2013 Abstract T43A-2622 presented at 2013 Fall Meeting, AGU, San Francisco, Calif., 9-13 Dec.

Scharer, K. M., T. E. Fumal, R. J. Weldon II, and A. R. Streig (2015), Photomosaics and event evidence from the Frazier Mountain paleoseismic site, trench 1, cuts 5–24, San Andreas Fault Zone, southern California (2010–2012), U.S. Geol. Surv. Open File Rep., 25 p., 3 sheets, doi:10.3133/ofr20151147.

Seeber, L., and Armbruster, J.G., 1995, The San Andreas Fault system through the Transverse Ranges as illuminated by earthquakes: Journal of Geophysical Research, v. 100, no. B5, p. 8285–8310, doi: 10.1029/94JB02939.

Stone, J., 2004. Extraction of Al and Be from Quartz for Isotopic Analysis. In: UW Cosmogenic Nuclide Lab Methods and Procedures. URL: http://depts. washington.edu/cosmolab/chem.html.

Sykes, L.R., and Seeber, L., 1985, Great earthquakes and great asperities, San Andreas fault, Southern California: Geology, v. 13, p. 835–838, doi: 10.1130/0091-7613(1985)13 2.0.CO;2.

Sylvester, A.G., and Smith, R.R., (1976) Tectonic transpression and basement-controlled deformation in the San Andreas fault zone, Salton trough, California, American Association of Petroleum Geologists, v. 60, pp. 74-96.

Vaughan, F. E., 1922, Geology of the San Bernardino Mountains north of San Gorgonio Pass [California]: California Univ. Dept. Geol. Sci. Bull., v. 13, no. 9, p. 319-411.

Wolff, L. R., and Yule, D. 2014. Reconciling contradicting trench and geomorphologic observations across the San Gorgonio Pass Fault Zone, Abstract 2014 at SCEC annual meeting, Palm Springs, Ca Sep 6-10.

Yule, D., McBurnett, P., and Ramzan, S., 2011, Long Return Periods for Earthquakes in San Gorgonio Pass and Implications for Large Ruptures of the San Andreas Fault in Southern California, Abstract T21A-xx at 2011 Fall Meeting, AGU, San Francisco, 5-9 Dec.

Yule, D., & Sieh, K. (2003). Complexities of the San Andreas fault near San Gorgonio Pass: Implications for large earthquakes, *108*. http://doi.org/10.1029/2001JB000451

APPENDIX A: TABLES

Table 1: Unit descriptions

Qf1	• Cobble conglomerate, with common boulders. Occasional fining upward sequences centimeters in width. • Moderately indurated. • Clasts are subrounded to sub angular. • Matrix is made up of medium to coarse sand, with some silt. • the top is defined by a distinct bright yellow to orange paleosol found throughout entire field area. • Paleosol is more indurated and protrudes from the canyon walls enough to define the boundary well. • Sediment is a greyish tan color in general with the exception of the paleosol. • Oldest visible unit, exposed due to uplift and shortening. • Induration is poor enough to have an extensive talus pile at the base of the canyon walls.
Qf2	• Contains a discontinuous light yellow paleosol. • conglomerate made up of mostly cobbles and gravel. With common boulders. • Matrix ranges from silt to coarse sand • Color of conglomerate is greyish tan • Youngest exposed unit, also uplifted and shortened from original height and length. • matrix ranges from silt to coarse sand • Moderately indurated, more so than Qf1. • Talus piles are mostly likely made up of both Qf1 and Qf2 • The base of this unit is above well-defined lower paleosol • Top of the unit is below alluvial terrace soil that blankets the surfaces of most of the field area

Table 2: Compilation of Qf2 ages from previous studies

Study	**Method**	**Age (of Qf2)**
Kendrick et al., 2015	Soil-profile development	106-130 ka
Owen et al., 2014	^{10}Be terrestrial cosmogenic radionuclide (TCRN)	40-75 ka
N. Lifton (personal communication)	^{10}Be/^{26}Al Cosmogenic Nuclide Isochron burial dating	330-510 ka
This Study	Preferred age (see discussion in text)	120-230 ka

Table 3: Fan 1 and Garnet Hill strand deformation rates

	Motion	**Offset**	**Age**	**Rates**
F1 deformation	**Uplift**	370 m +/- 30	120-230 kyr	1.5-3.3 mm/yr
	Shortening	400 m +/- 40	120-230 kyr	1.6-3.7 mm/yr
Garnet Hill strand	**Uplift**	8+/- 1	5.65+/- 1.05	1.0-1.8 mm/yr
Banning strand	**Dextral**	1.5-2.7 km	120-230 kyr	7.0-23 mm/yr

APPENDIX B: FIGURE CAPTIONS

Figure 1: Fault map of part of southern California. Figure modified from Cooke and Dair (2011) and shows major fault systems and their locations in San Gorgonio Pass (SGP), Coachella Valley (CV), and the Eastern California Shear Zone (ECSZ). The San Andreas Fault system consists of the Mojave, San Bernardino, Mill Creek, San Gorgonio Pass, Garnet Hill, Banning, Mission/Mill, and Coachella strands. This study focuses on the stepover between the Banning and Garnet Hill/San Gorgonio Pass strands, San Andreas Fault, Whitewater, California (area marked by red box). CH – Crafton Hills; CP –Cajon Pass; TB – Timoteo Badlands; YR – Yucaipa Ridge.

Figure 2: Geologic map of west Whitewater Hill (WWH). Base map is from B4 LiDAR DEM image overlaid with topography lines (contour interval is 40 ft.) from USGS.org. Geologic units: PcK (olive green) – Precambrian to Cretaceous intrusive and metamorphic complex; Qf1 (green) – Pleistocene lower Cabazon fanglomerates; Qf2 (blue) – Pleistocene upper Cabazon fanglomerates, Qaf (orange) – Holocene faulted alluvium; Qau (yellow) – Holocene unfaulted alluvium; and Qs (mauve) – extensive orangish-red soil. Dark blue and green lines represent paleosols, PS2 and PS1, respectively. Red lines are faults (dashed where buried) with arrows and up-down (U or D) labels to indication sense of slip and/or separation. Black circles show locations of $^{10}Be/^{26}Al$ burial age date samples; black triangles denote locations of clast counts; short, thick, black lines with roman numerals near them show the stratigraphic column locations. Box shows area of Figure 3.

Figure 3: Unit stratigraphy of West Whitewater Hill. All of the units mapped within West Whitewater Hill listed and described in chronological order, from oldest at the bottom to youngest at the top.

Figure 4: Tortoise burrow in unit PcK and gouge zone along Banning strand, SAF. Unit PcK granites and gneisses have been so destroyed in the crush zone of the Banning strand that a tortoise made its home there rather than the less indurated Quaternary fan units south of the fault.

Figure 5: N-S trending secondary faults. Field photo of J. Cardona and B. Huerta standing on either side of an unnamed secondary fault along the top of West Whitewater Hill. The view is looking to the east, with up being on the east and down on the west. We interpret the motion on the fault to be reverse.

Figure 6: Cross section A-A'. See Figure 2 for line of section and unit explanation. Section is orthogonal to south-plunging fold and shows steep-dipping secondary reverse faults in core of fold. Fault at west is the north splay of the Garnet Hill strand. Whitewater Canyon is on the east; Cottonwood Canyon is on the west. Total structural relief across fold is about 300 m, and total shortening is about 400 m. Dashed lines show where a unit or contact is assumed to be; red lines show faults and their motion.

Figure 7: Cross section B-B'. See Figure 2 for line of section and unit explanation. Section is orthogonal to strikes of Banning and Garnet Hill strands. Note that unit Qs occurs at about the same elevation on either side of the Banning strand due nearly pure dextral slip on this fault. Southern two faults are splays of the dextral-oblique Garnet Hill strand. Dashed lines show where a unit or contact is assumed to be; red lines show faults and their motion.

Figure 8: Pie diagram of clast counts in unit Qf1. results from locations within Qf1. These were taken for comparison to the modern clasts found on the west and east side of the canyon.

Figure 9: Stratigraphic columns. For locations see Figure 2. Columns are arranged relative to elevation. Unit colors and abbreviations are same as shown in Figure 2.

Figure 10: Fence diagram of stratigraphic columns. Datum is unit Qs. Columns arranged from west to east show decreasing thickness of unit Qf2 toward the east and Whitewater Canyon. Refer to Figure 11 for contoured isopach map of Qf2 thicknesses.

Figure 11: Contoured isopach map of unit Qf2. Base is topographic map with 40 ft. topographic contour interval. Thickness estimate of unit Qf2 are given by 10 m contour interval. Control for isopach thickness is shown by black dots where thickness between paleosol 1 and soil Qs are exposed in canyon walls. Contours define a fan apex at the top

of west Whitewater hill. The fan apex appears to be beheaded by the Banning strand, and shows a dextral offset of 2.2-3.0 km.

Figure 12: Modern Whitewater River fan. Image taken from Google Earth Pro. View of West Whitewater Hill and Whitewater River. Major faulting is shown is red lines with arrows showing dextral motion and up and down showing areas of reverse slip. Modern Whitewater River and its modern alluvial fan are outlined in black. Modern Whitewater fan here is a proxy for the ancestral Qf2 fan that was offset by the Banning strand.

Figure 13: Pie diagrams of clast counts in unit Qau. from both sides of west Whitewater hill. One is from the modern Whitewater River drainage and the other was taken from Cottonwood Canyon.

Figure 14: Geologic map of offsets along splays of Garnet Hill strand. Base is B4 LiDAR DEM image with sun angle from SW. Blue arrows point to scarps along north splay. Black arrows point to 1-2 m-high scarps on south splay. Yellow arrows point to lateral offset features (streams and/or terrace edges). Areas in orange is unit Qs (see text and caption for Figure 2). Note that the Colorado River Aqueduct tunnels under the eastern part of the map area.

Figure 15: Map extent of alluvial fan surfaces. LiDAR and topo base, and fault are same as shown in Figure 2. The oldest is fan surface F1 (mauve) and is recognized by unit Qs

where developed on unit Qf2. Young fan surfaces are fan surfaces F2 (orange) and F3 (yellow) and represent surfaces to units Qaf and Qau, respectively. See text for correlation of these features with those described in Owen et al., 2014.

APPENDIX C: FIGURES

Figure 1: Fault map of part of southern California

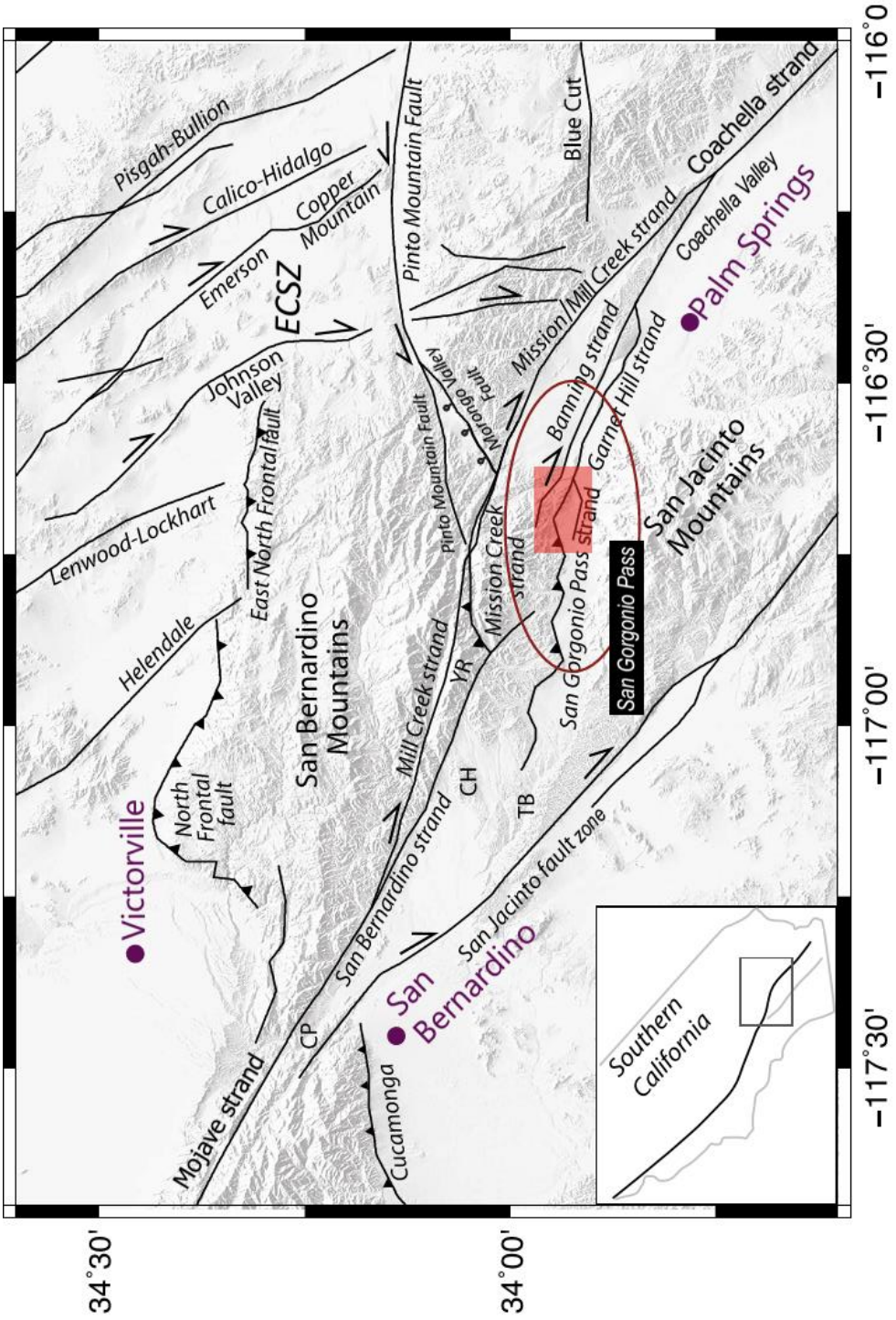

Figure 2: Geologic map of West Whitewater Hill (WWH)

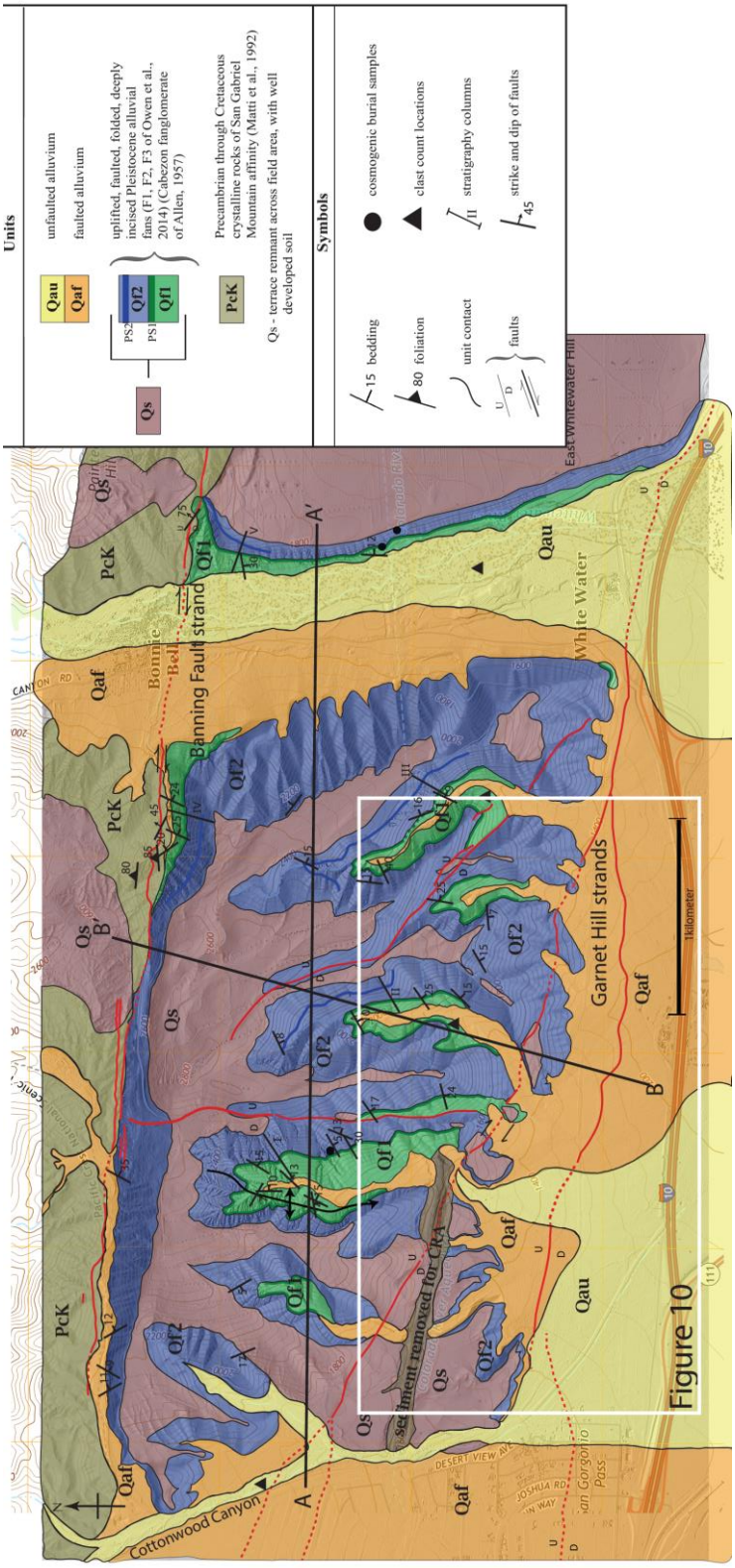

Figure 3: Unit Stratigraphy of West Whitewater Hill

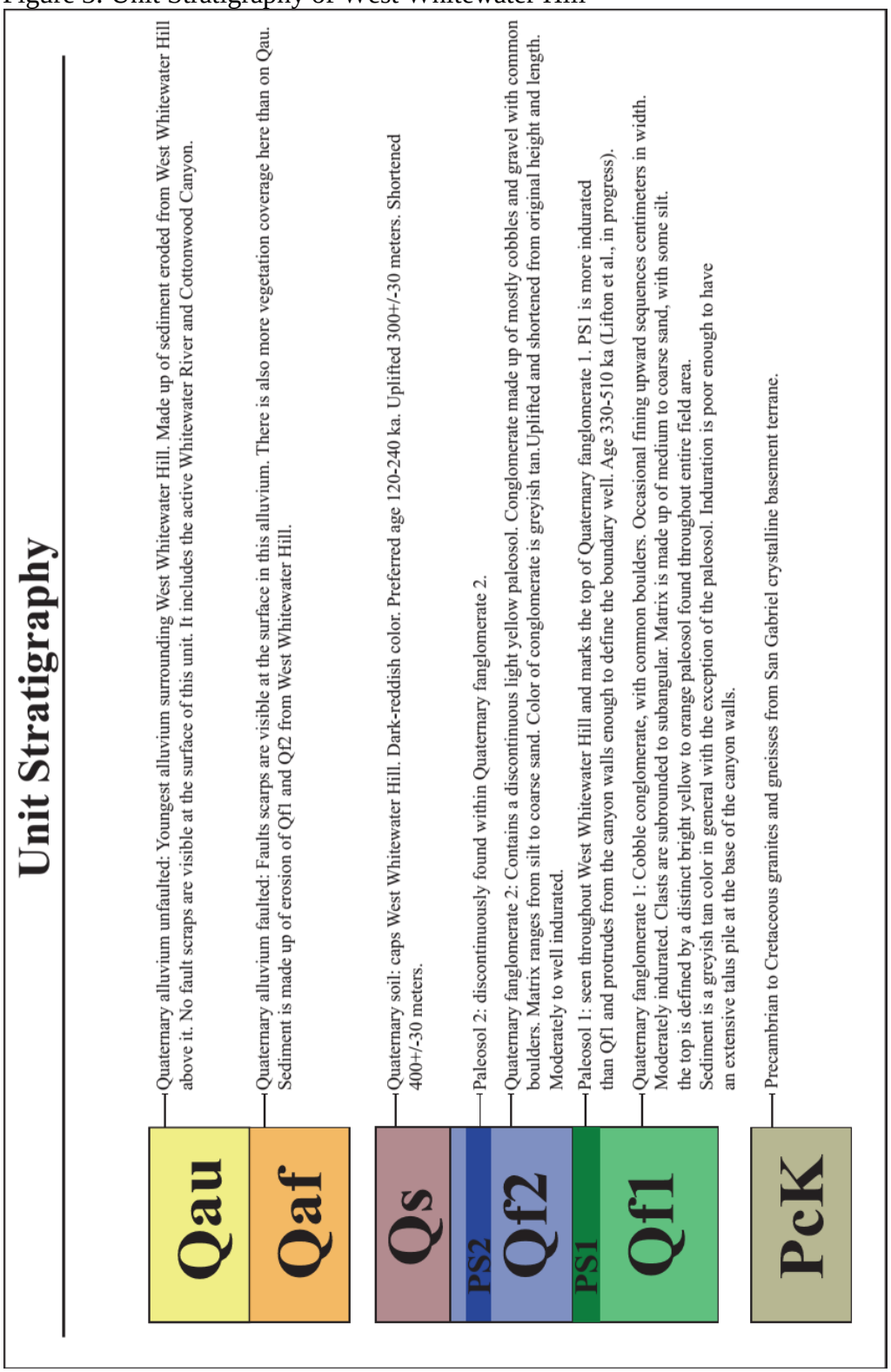

Figure 4: Tortoise burrow in PcK gouge zone of Banning strand SAF.

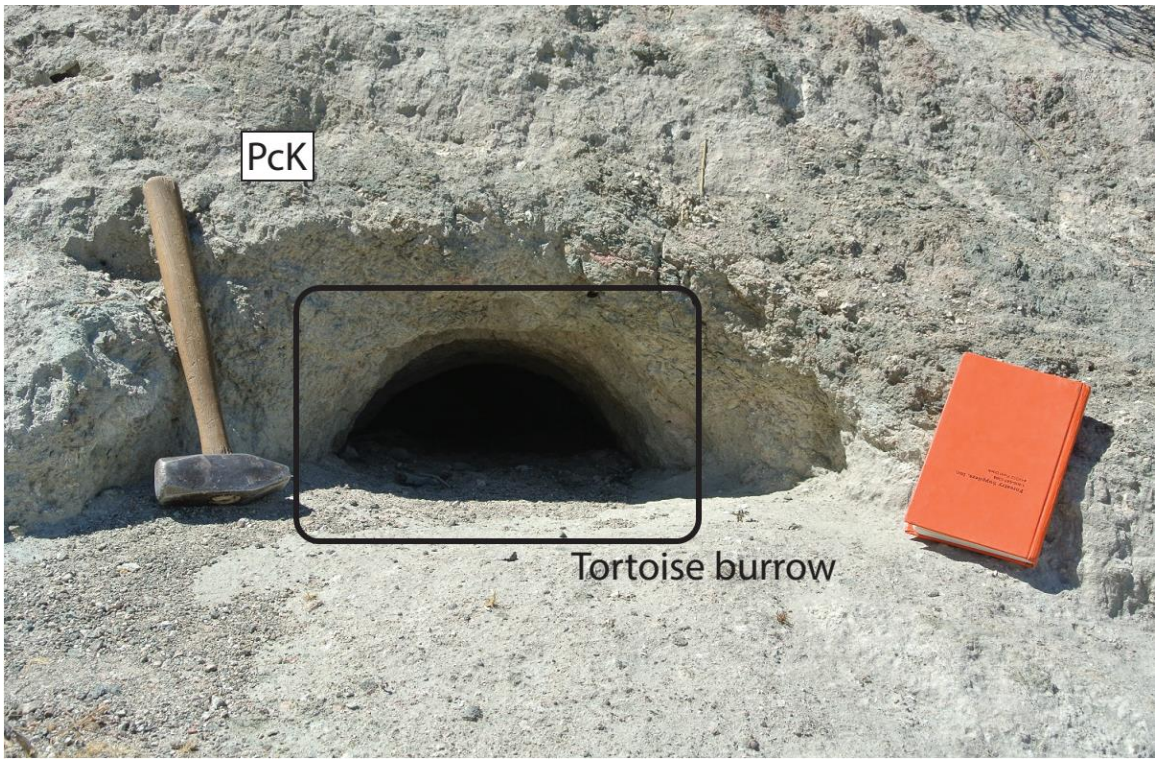

Figure 5: N-S trending secondary faults

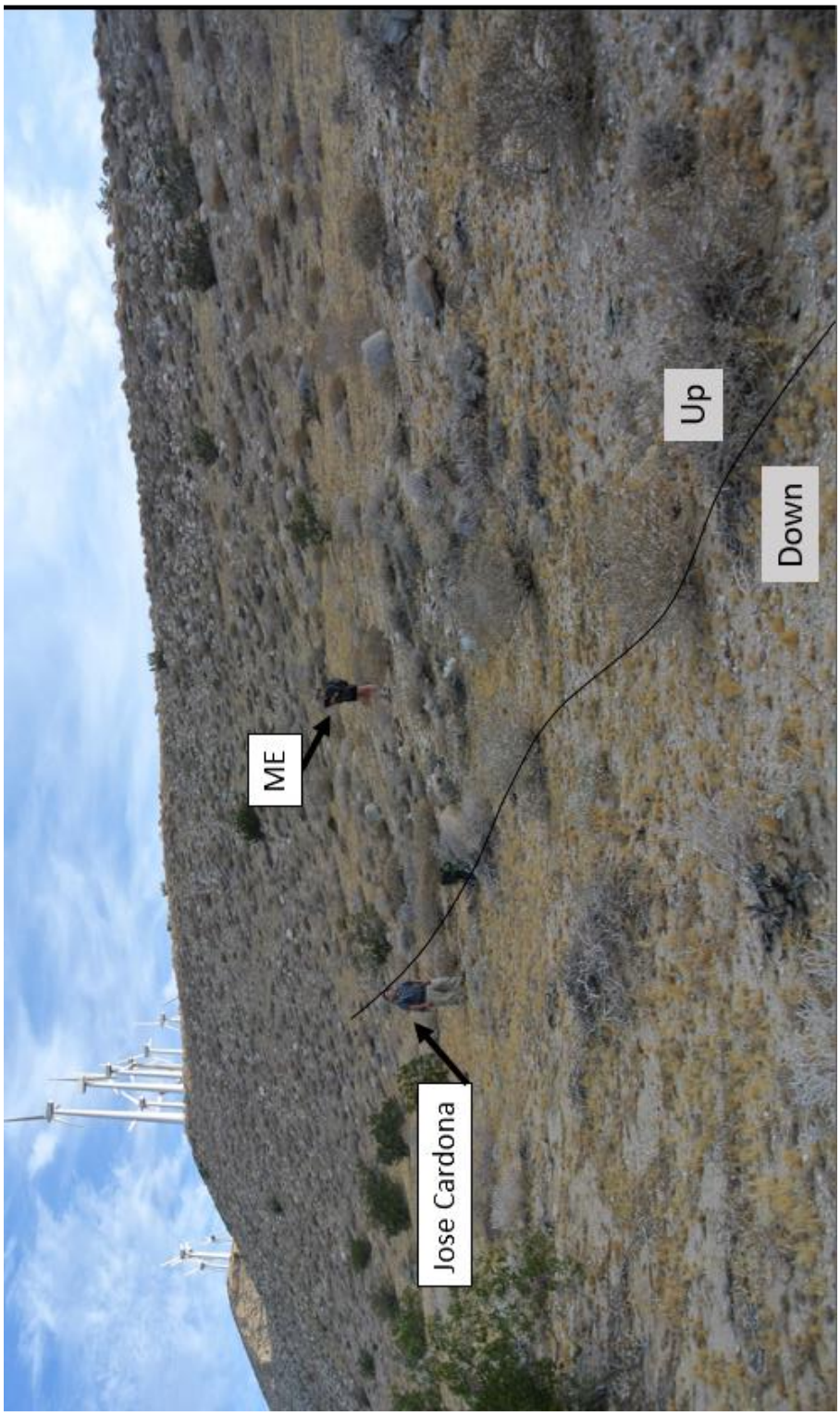

Figure 6: Cross section A-A’

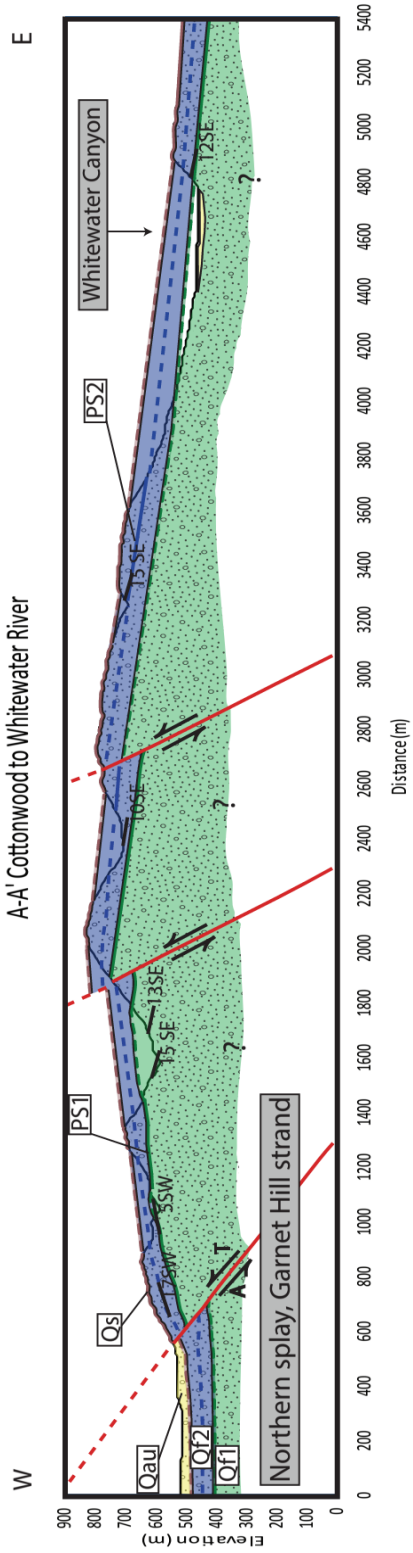

Figure 7: Cross section B-B’

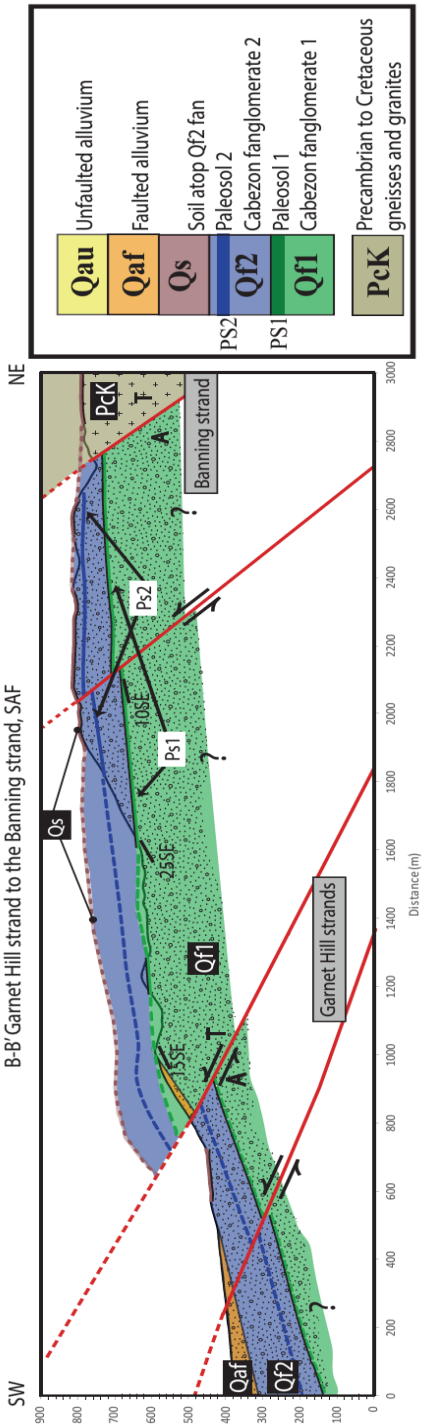

Figure 8: Pie diagram of clast counts in unit Qf1

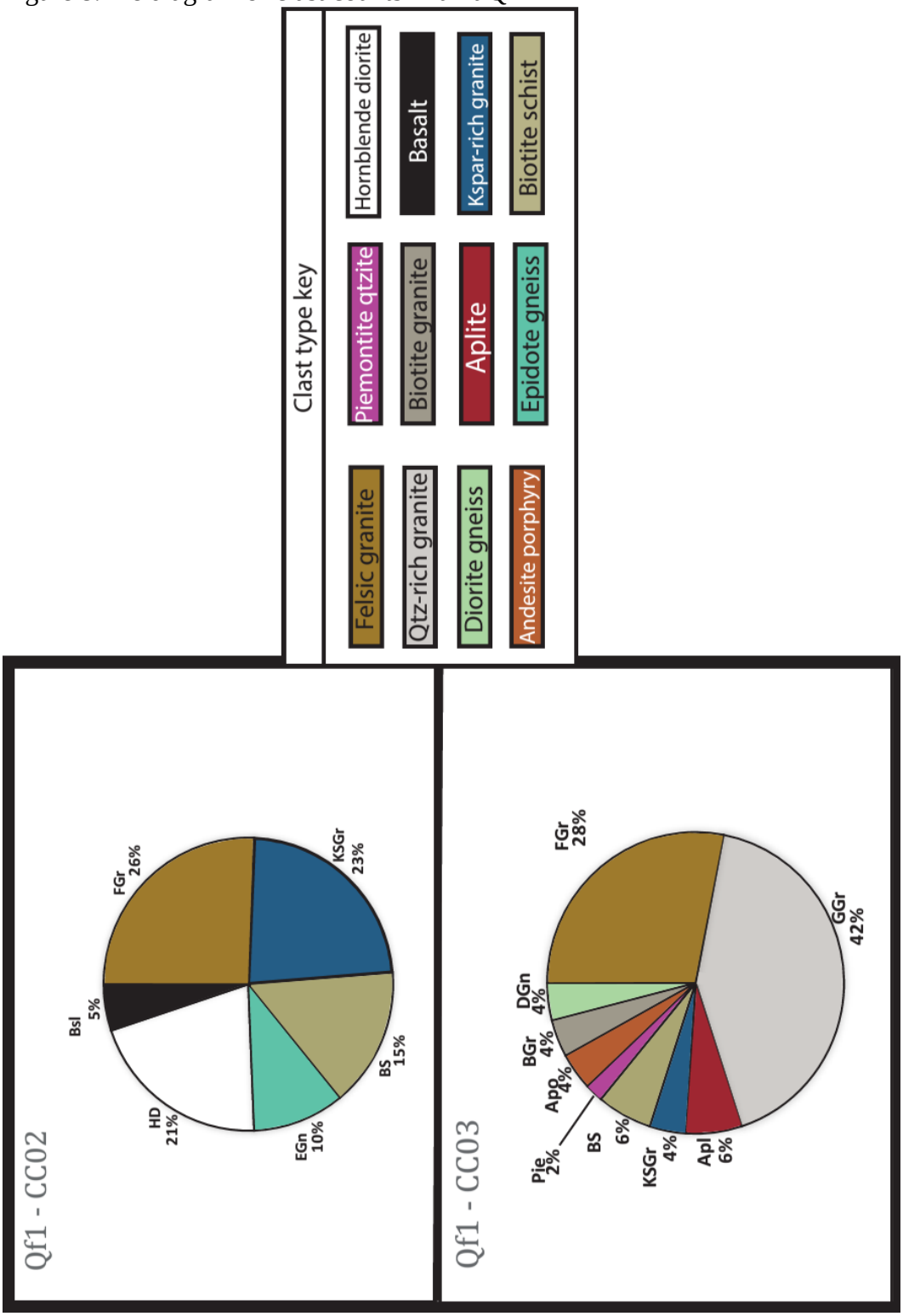

Figure 9: Stratigraphic columns

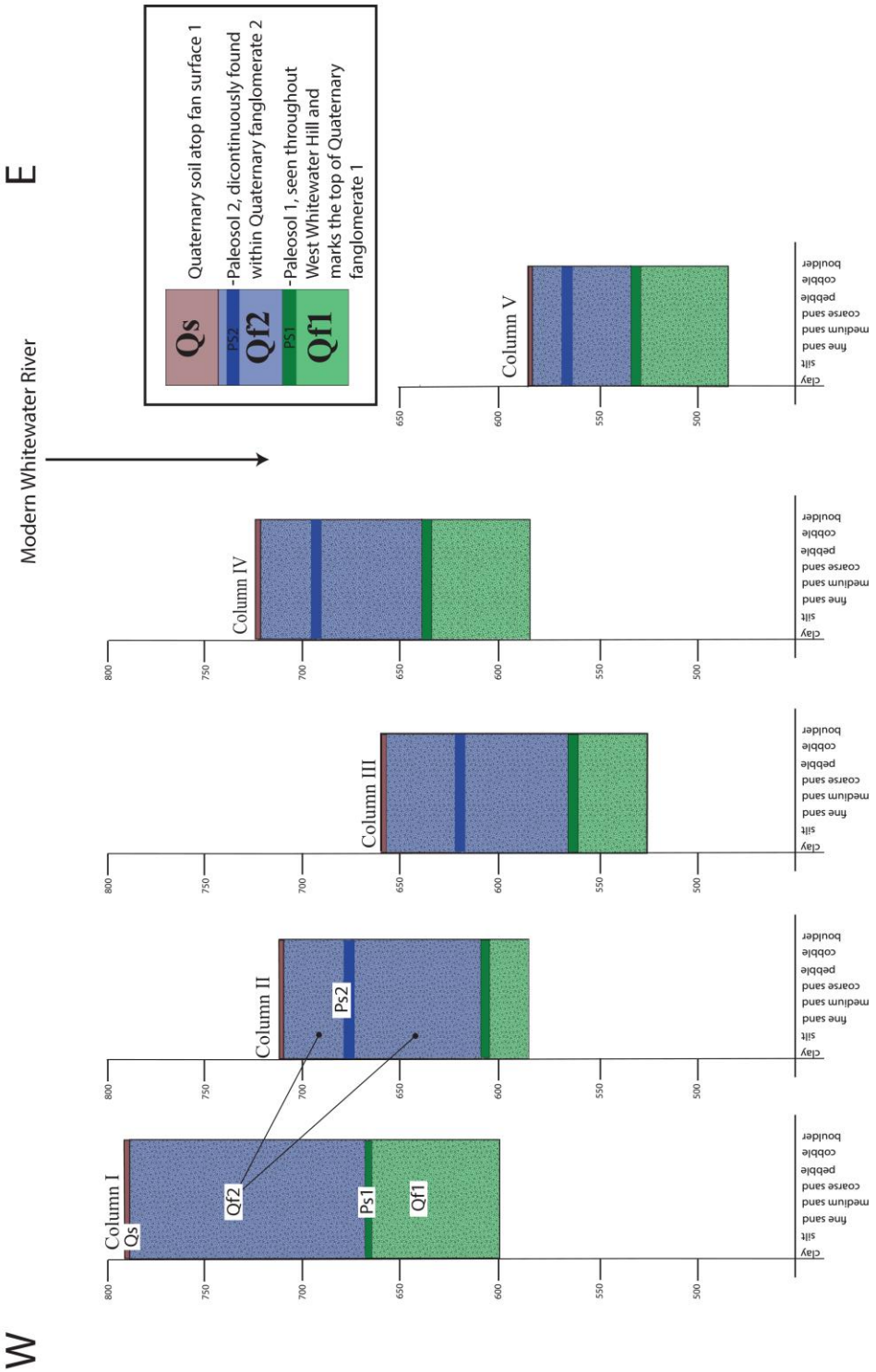

Figure 10: Fence diagram of stratigraphic columns

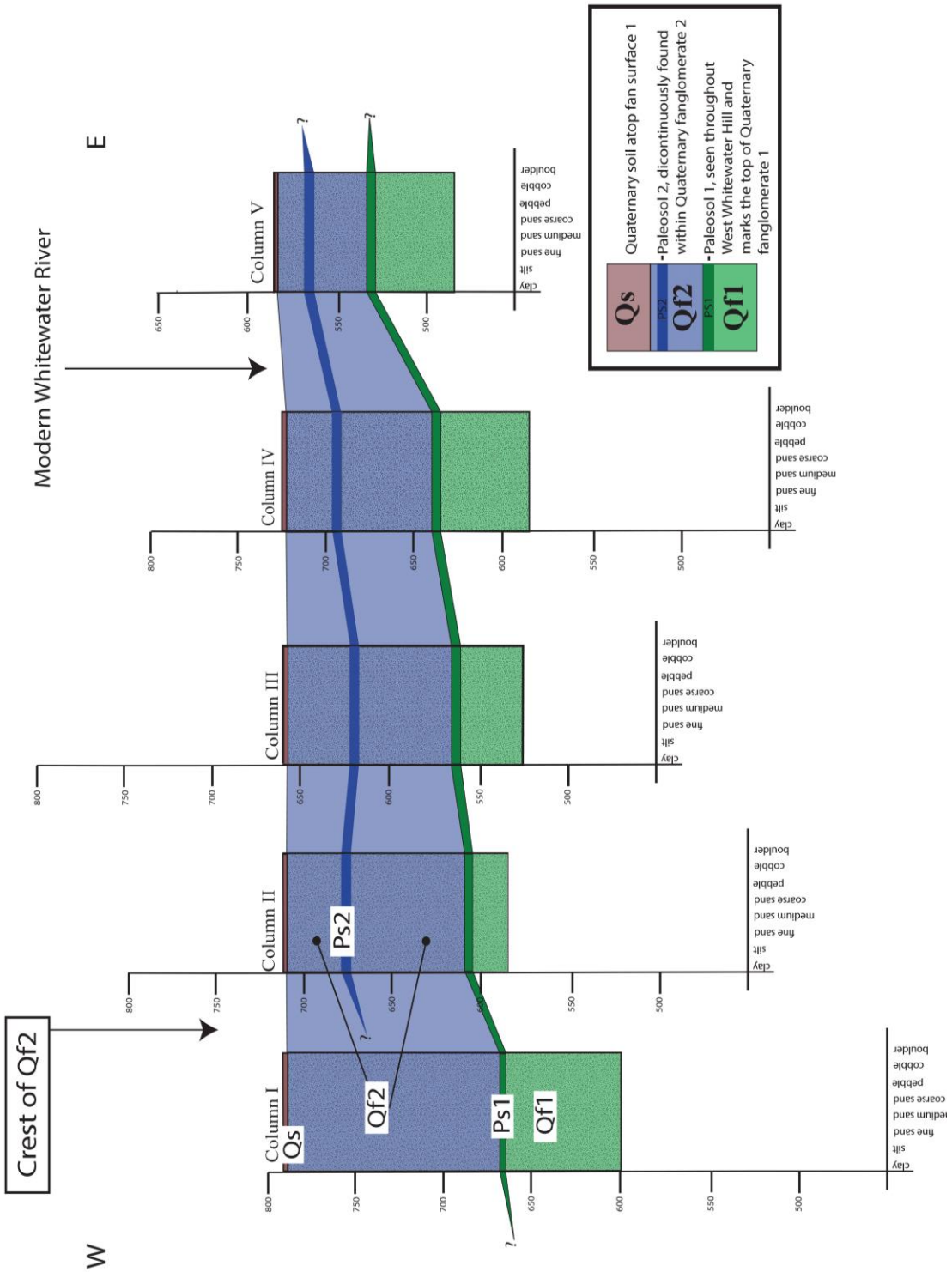

Figure 11: Contoured isopach map of unit Qf2

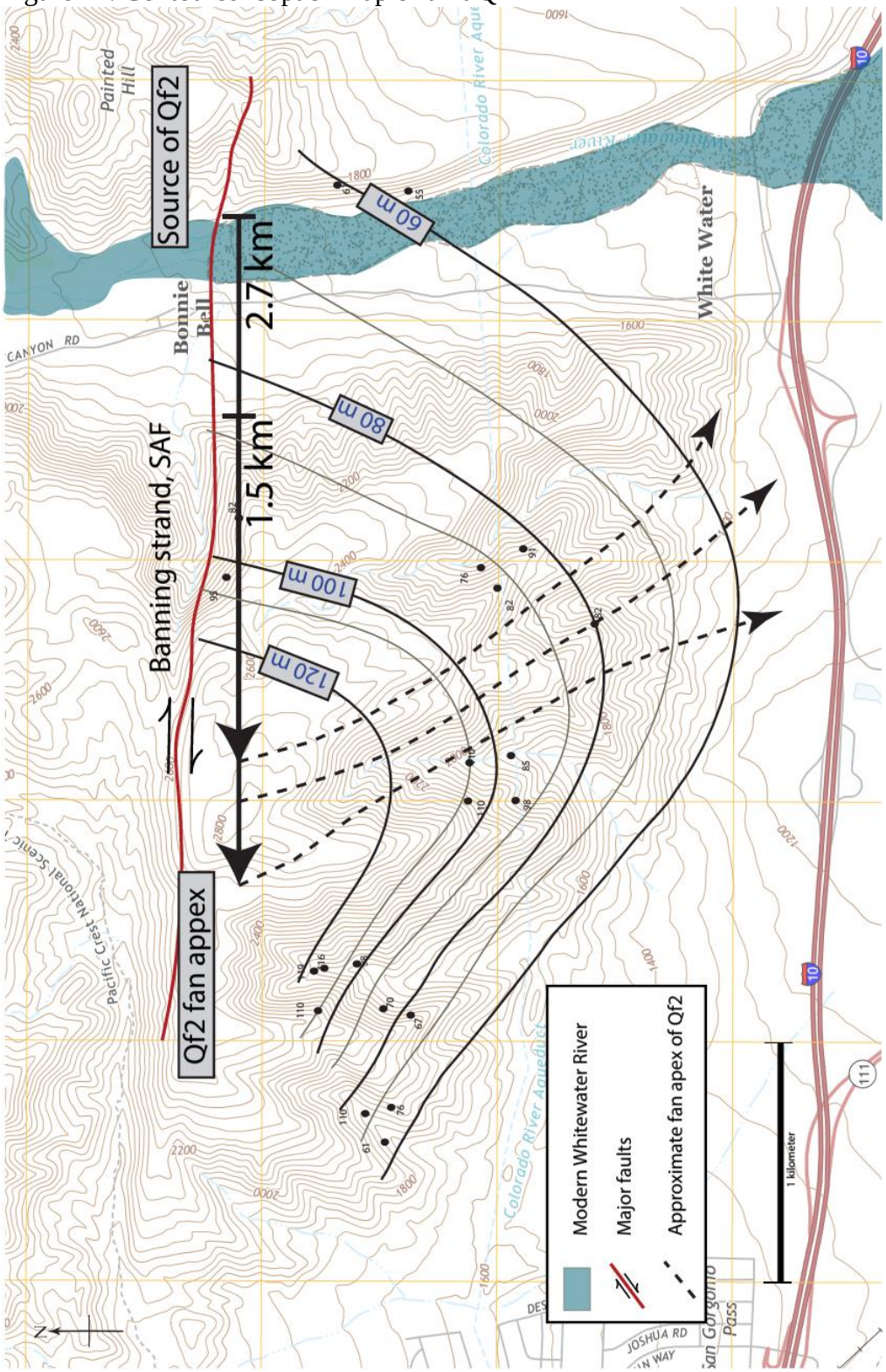

Figure 12: Modern Whitewater River fan

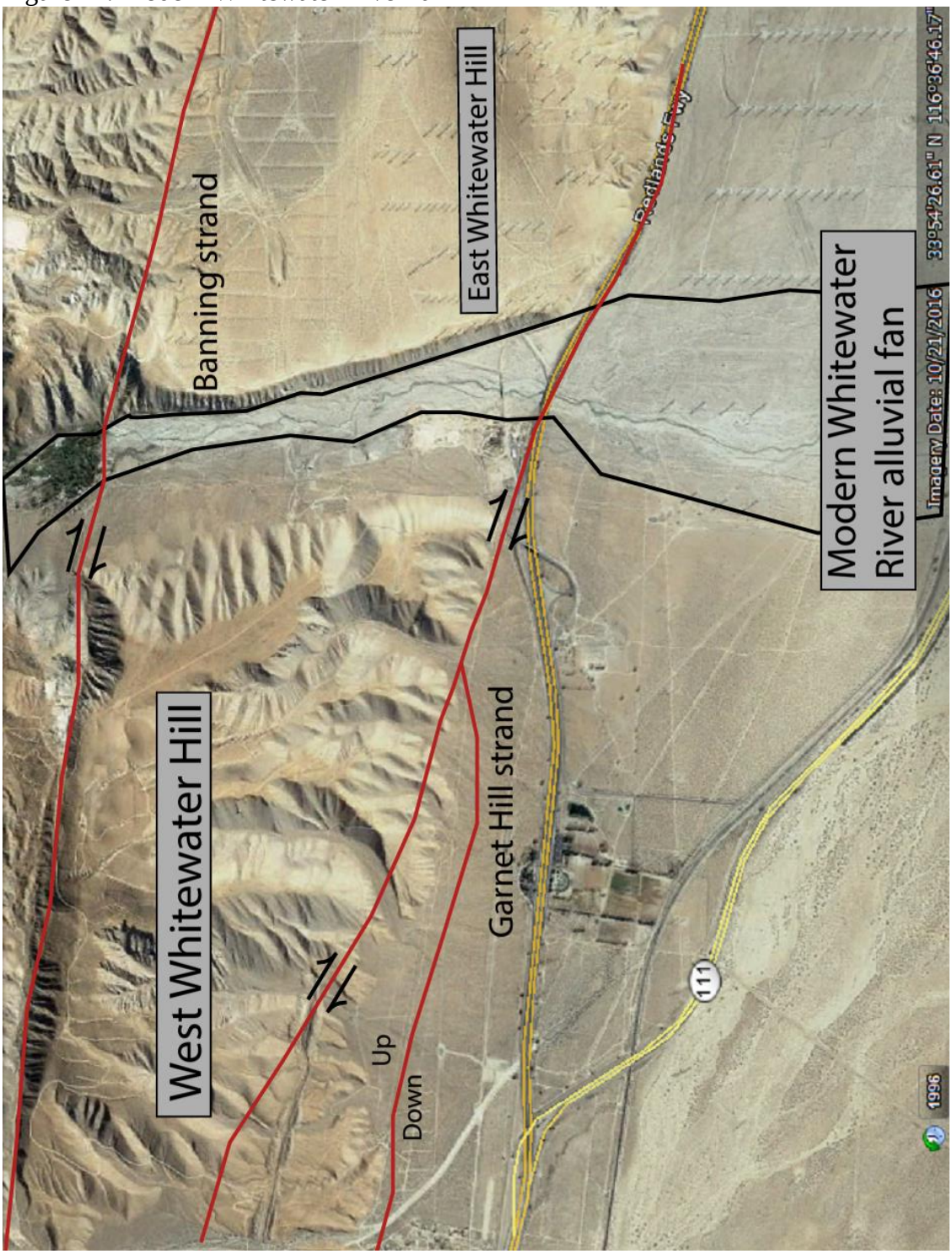

Figure 13: Pie diagrams of clast counts in unit Qau

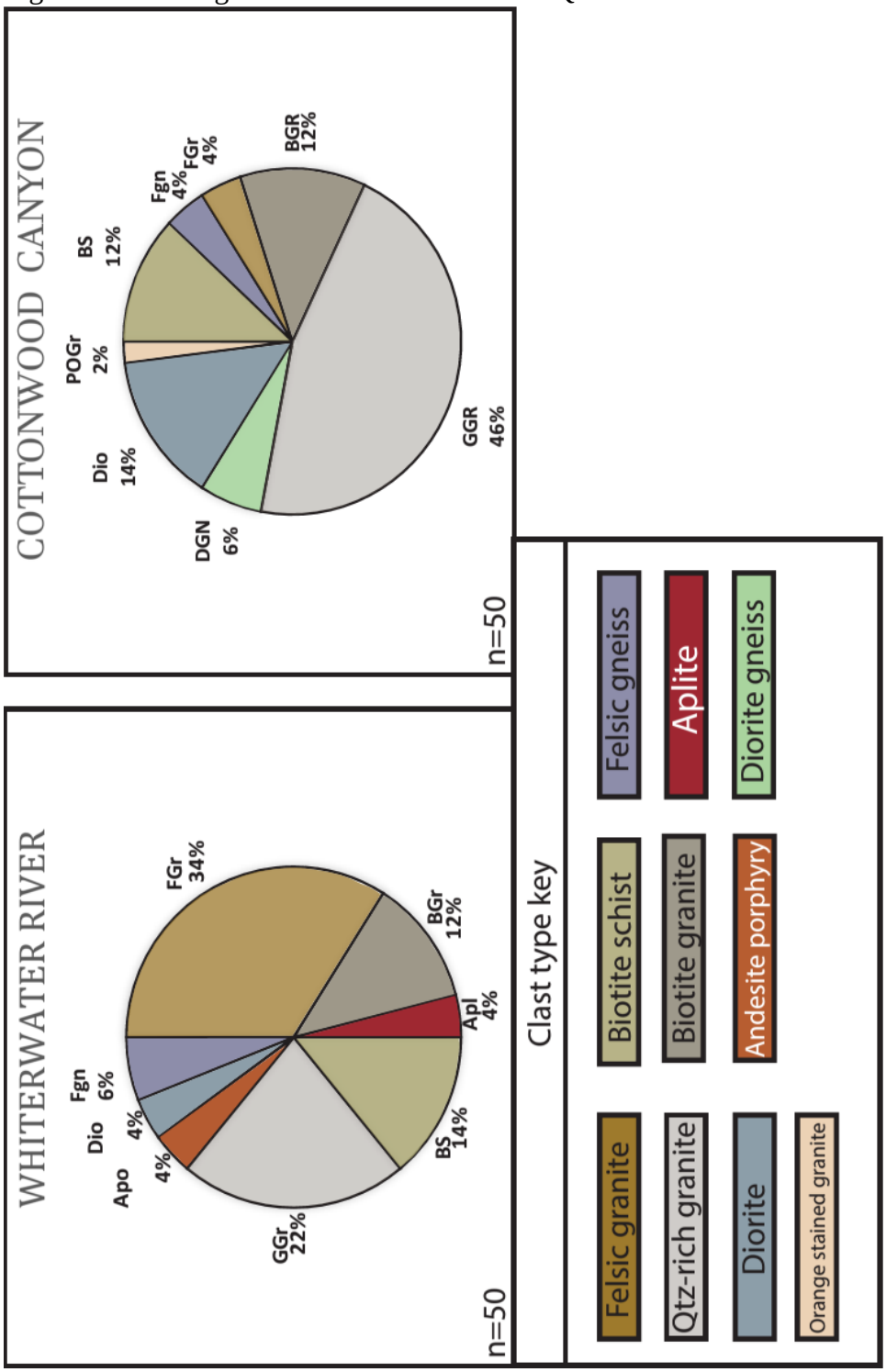

Figure 14: Geologic map of offsets along splays of Garnet Hill strand

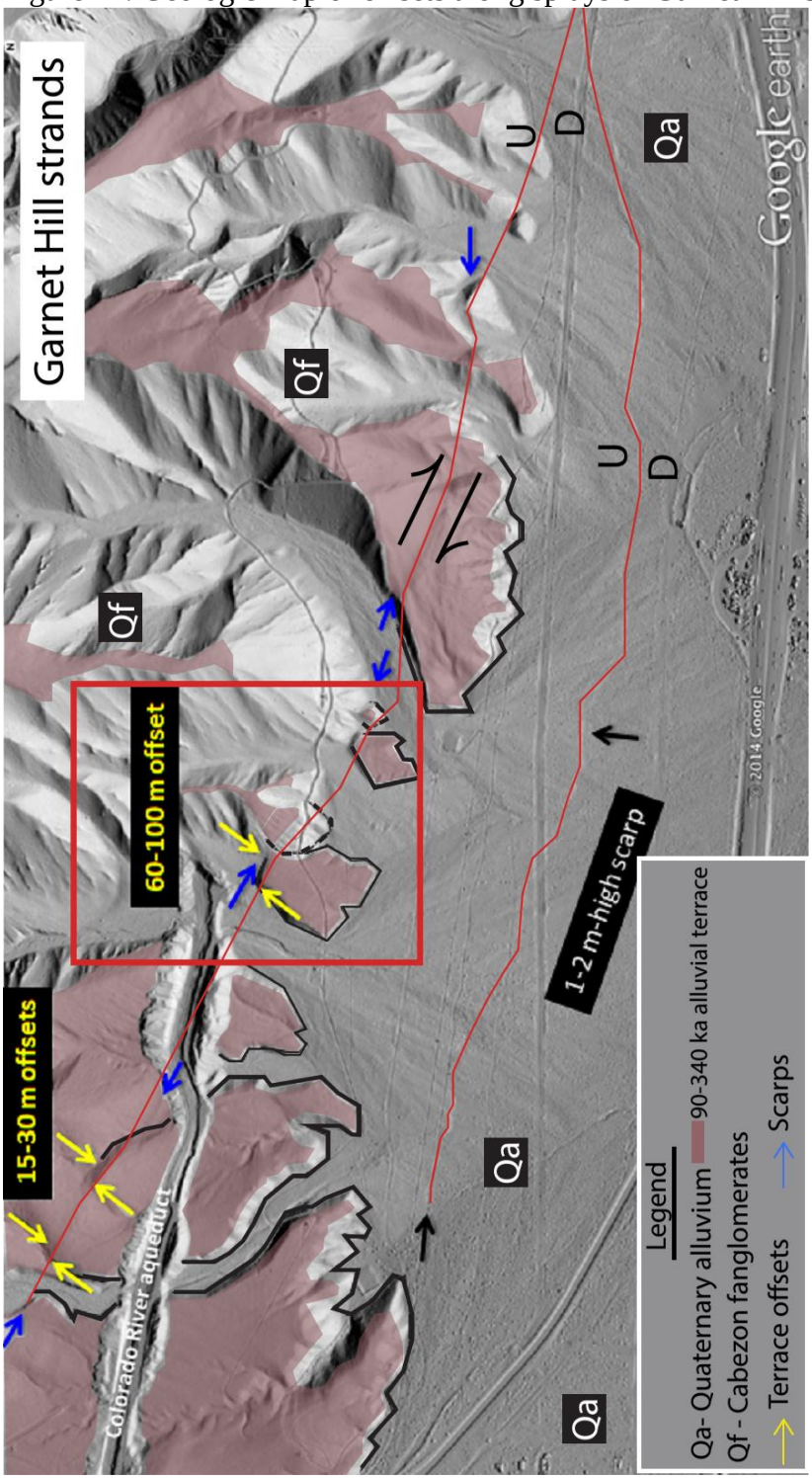

Figure 15: Map extent of alluvial fan surfaces

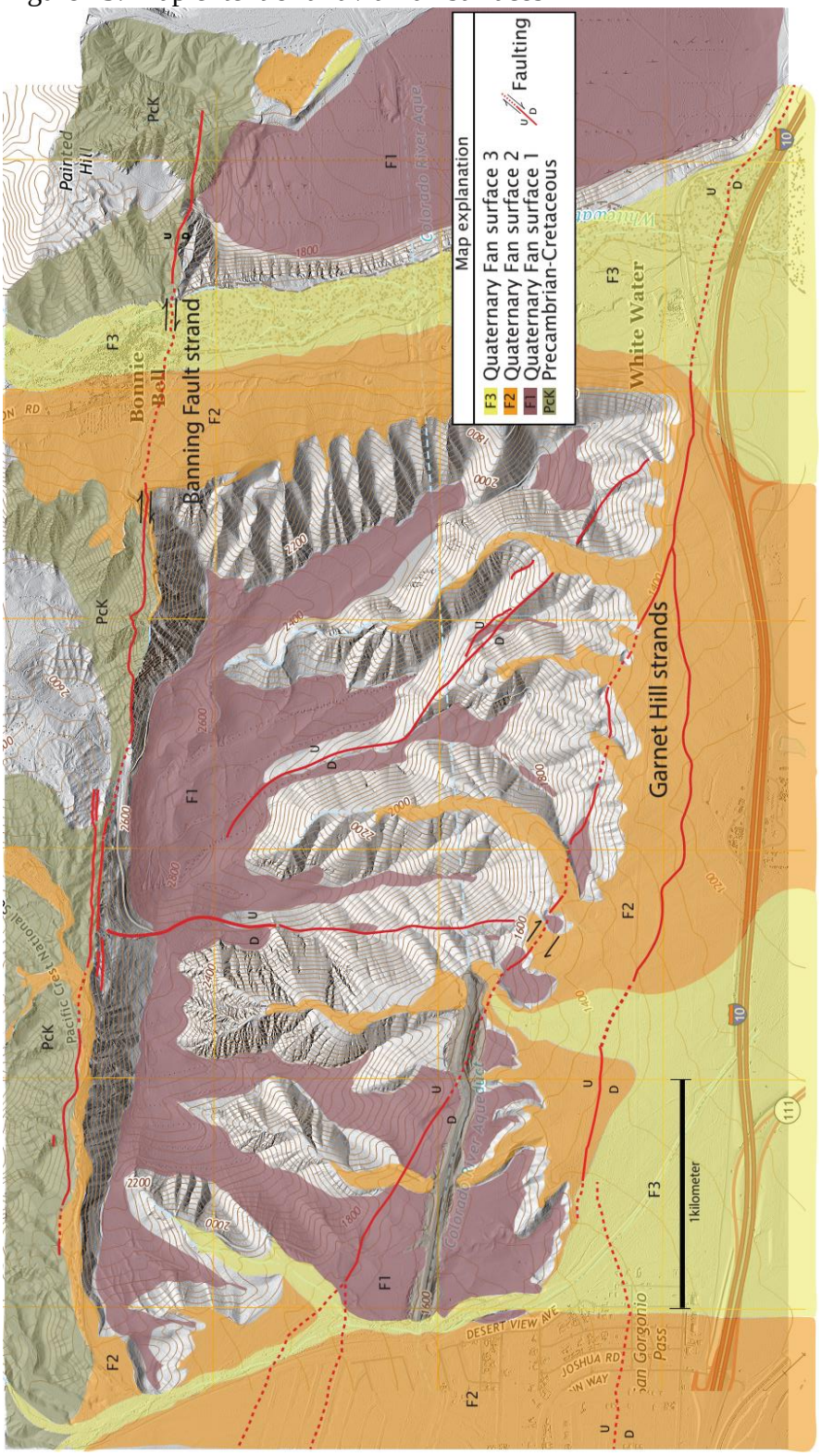

APPENDIX D

Collected trend/plunge and calculated strike/dip	**Eigenvalue**	**Trend**	**Plunge**
Data set: point 2 and 3			
1	0.7494	105.0,	2.3
2	0.2506	195.1,	4
3	0	345.0,	85.4
Best fit great circle (strike, dip RHR) = 075.0, 04.6			
Data set: point 12			
1	0.7555	140.3,	11.5
2	0.2445	049.1,	6
3	0	292.1,	77
Best fit great circle (strike, dip RHR) = 022.1, 13.0			
Data set: point 13			
1	0.9139	152.4,	13.6
2	0.0861	243.2,	3.3
3	0	346.7,	76
Best fit great circle (strike, dip RHR) = 076.7, 14.0			
Data set: 21/22/23			
1	0.811	172.5,	15.2
2	0.1879	079.7,	10.2
3	0.0011	316.9,	71.6
Best fit great circle (strike, dip RHR) = 046.9, 18.4			
Data set: 21/22/23			
1	0.8482	165.7,	14.9
2	0.1486	073.4,	8.6
3	0.0033	314.5,	72.7
Best fit great circle (strike, dip RHR) = 044.5, 17.3			
Data set: pt 33			
1	0.7145	122.4,	7.7
2	0.2855	212.8,	2.8
3	0	322.6,	81.8
Best fit great circle (strike, dip RHR) = 052.6, 08.2			
Data set: pt 38			
1	0.7518	129.8,	7.5
2	0.2482	220.5,	5
3	0	343.9,	81
Best fit great circle (strike, dip RHR) = 073.9, 09.0			

Collected trend/plunge and calculated strike/dip	**Eigenvalue**	**Trend**	**Plunge**
Data set: pt 38			
1	0.7518	129.8,	7.5
2	0.2482	220.5,	5
3	0	343.9,	81
Best fit great circle (strike, dip RHR) = 073.9, 09.0			
Data set: pt 53			
1	0.9545	153.2,	10.9
2	0.0448	062.4,	4.1
3	0.0007	312.0,	78.3
Best fit great circle (strike, dip RHR) = 042.0, 11.7			
Data set: pt 54			
1	1	115.0,	16
2	0	025.0,	0
3	0	295.0,	74
Best fit great circle (strike, dip RHR) = 025.0, 16.0			
Data set: pt 56			
1	0.6795	180.2,	11.5
2	0.3205	089.6,	2.6
3	0	347.1,	78.2
Best fit great circle (strike, dip RHR) = 077.1, 11.8			
Data set: pt 71			
1	0.9921	065.0,	13.5
2	0.0079	330.9,	16.7
3	0	192.2,	68.3
Best fit great circle (strike, dip RHR) = 282.2, 21.7			
Data set: pt 76 east			
1	0.9981	022.5,	10.5
2	0.0019	114.6,	11.3
3	0	250.6,	74.5
Best fit great circle (strike, dip RHR) = 340.6, 15.5			
Data set: pt 77 east			
1	0.97	150.0,	7.1
2	0.03	059.3,	5.7
3	0	290.7,	80.8
Best fit great circle (strike, dip RHR) = 020.7, 09.2			

Collected trend/plunge and calculated strike/dip	**Eigenvalue**	**Trend**	**Plunge**
Data set: pt 78 east			
1	0.8899	045.5,	6.9
2	0.1101	315.3,	1.5
3	0	213.1,	82.9
Best fit great circle (strike, dip RHR) = 303.1, 07.1			
Data set: pt 77 west			
1	0.99	235.1,	12
2	0.01	137.7,	30.8
3	0	343.8,	56.4
Best fit great circle (strike, dip RHR) = 073.8, 33.6			
Data set: pt 78 west			
1	0.9872	017.5,	4
2	0.0128	277.9,	67.2
3	0	109.2,	22.4
Best fit great circle (strike, dip RHR) = 199.2, 67.6			
Data set: pt 79			
1	0.9704	100.0,	8.6
2	0.0296	190.4,	2.9
3	0	298.7,	80.9
Best fit great circle (strike, dip RHR) = 028.7, 09.1			
Data set: pt 80			
1	0.8522	092.7,	7
2	0.1478	001.5,	9.1
3	0	219.9,	78.5
Best fit great circle (strike, dip RHR) = 309.9, 11.5			
Data set: pt 85			
1	0.8833	100.1,	8
2	0.1167	009.1,	7.3
3	0	237.2,	79.2
Best fit great circle (strike, dip RHR) = 327.2, 10.8			
Data set: pt 86			
1	0.9569	237.5,	16.9
2	0.0431	146.8,	2.3
3	0	049.3,	73
Best fit great circle (strike, dip RHR) = 139.3, 17.0			

Collected trend/plunge and calculated strike/dip	**Eigenvalue**	**Trend**	**Plunge**
Data set: pt 89			
1	0.9349	215.2,	15.5
2	0.0651	122.0,	11.4
3	0	357.0,	70.6
Best fit great circle (strike, dip RHR) = 087.0, 19.4			
Data set: pt 89			
1	0.9349	215.2,	15.5
2	0.0651	122.0,	11.4
3	0	357.0,	70.6
Best fit great circle (strike, dip RHR) = 087.0, 19.4			
Data set: pt 93			
1	0.6243	127.7,	3.1
2	0.3757	037.2,	9
3	0	236.8,	80.5
Best fit great circle (strike, dip RHR) = 326.8, 09.5			

APPENDIX E

Figure B1: Sample collection with Dr. Nathaniel Lifton

Figure B2: <1 m scarp of the southern splay of the Garnet Hill strand

Figure B3: Sand lens within Qf2

Figure B4: View of West Whitewater Hill from San Jacinto Peak

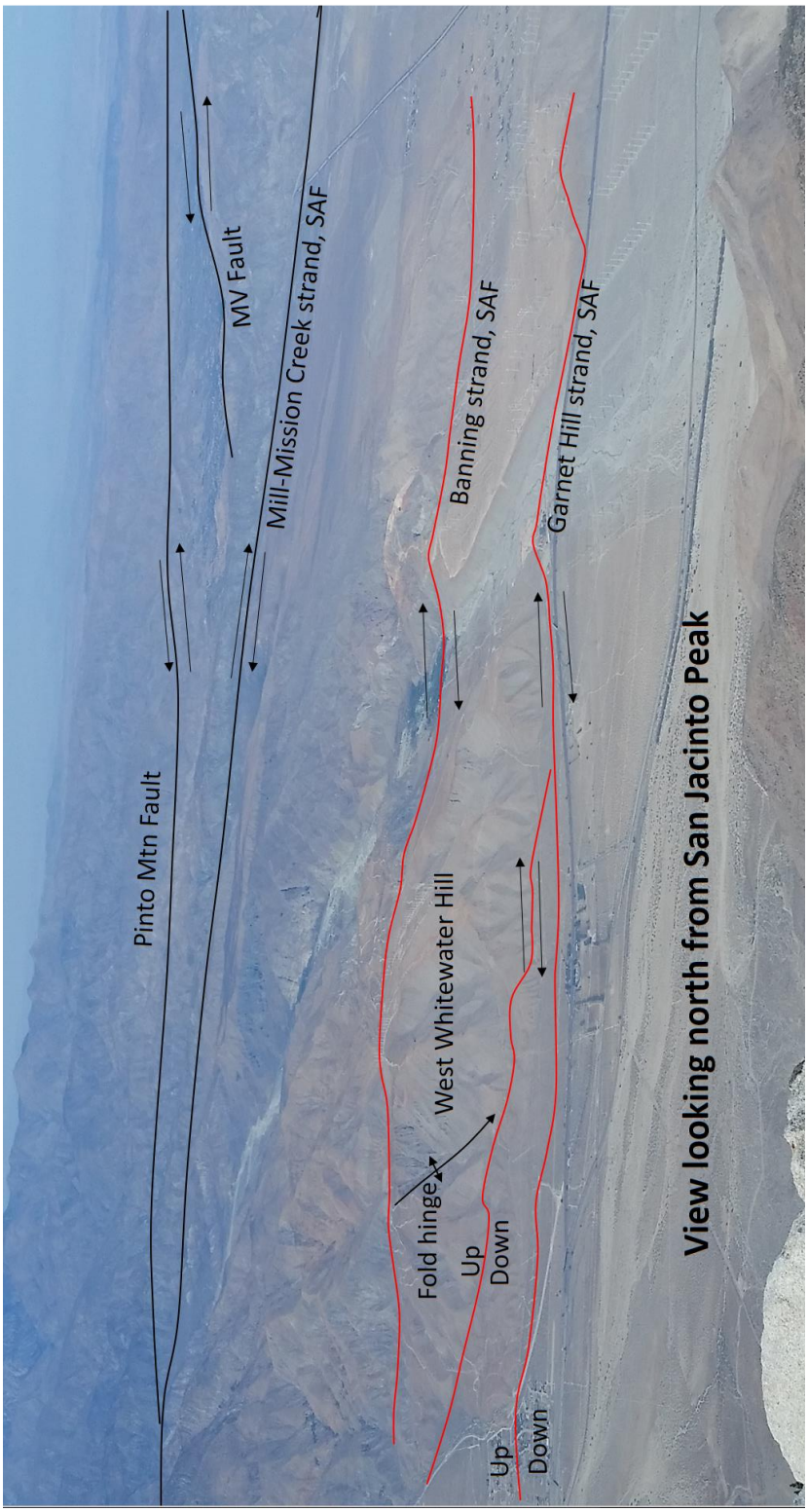

Figure B5: Steep canyon wall looking towards the west

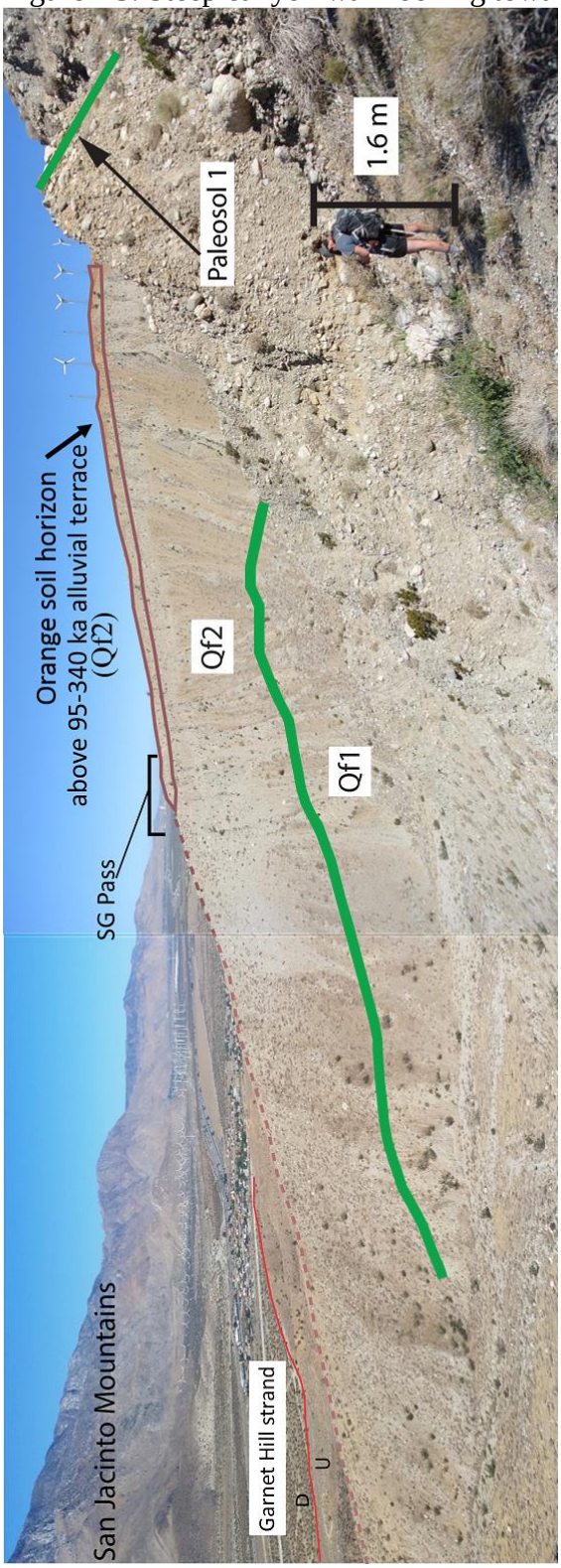

Figure B6: Paleosol 1 outcrop

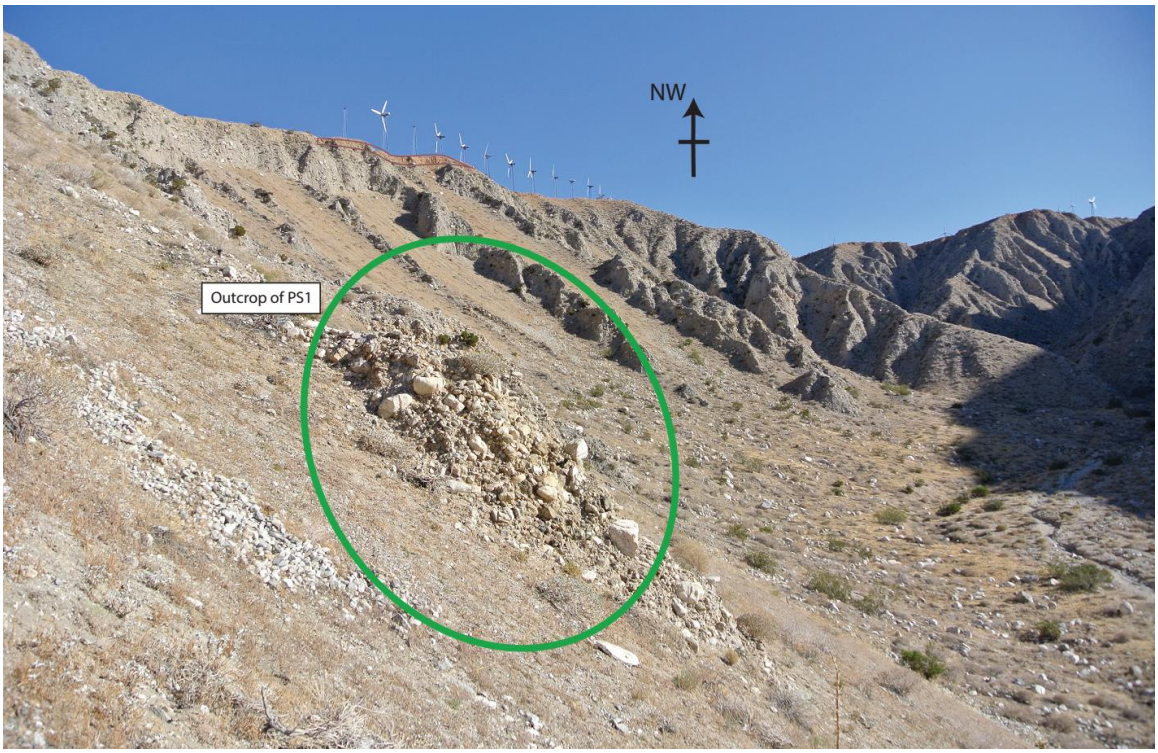

Figure B7: Northern Garnet Hill splay

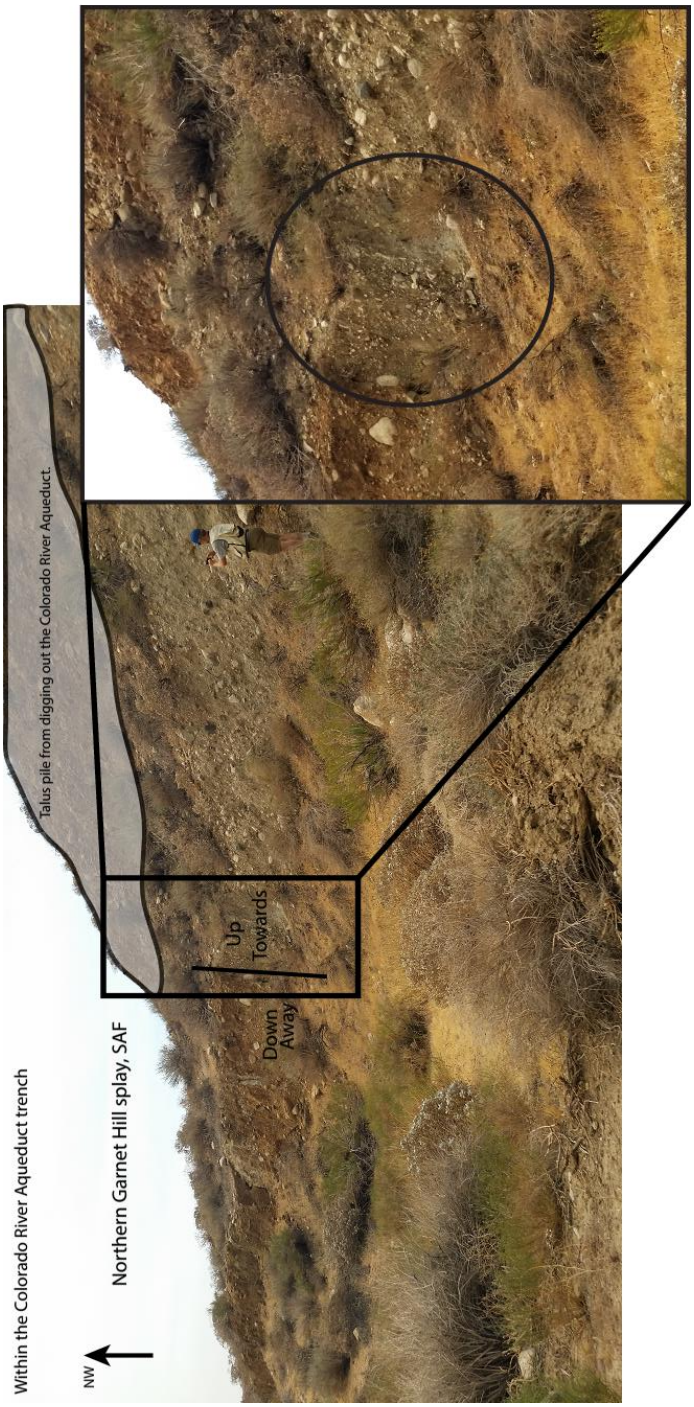

Figure B8: Uplift and shortening across West Whitewater Hill